https://doi.org/10.1016/j.engstruct.2021.111982

Tensile Behaviour of Headed Anchored Hollo-Bolts in Concrete Filled Hollow Steel Tube Connections

Partha Pratim DEBNATH and Tak-Ming CHAN*

Department of Civil and Environmental Engineering,

The Hong Kong Polytechnic University, Kowloon, Hong Kong

**tak-ming.chan@polyu.edu.hk*

Abstract

Achieving a strong and stiff bolted connection with concrete filled steel tube (CFST) has been a challenge to structural engineers, and therefore to enhance the connection performance, blind-bolts that are extended to anchor in the concrete core have been recently developed. Though some experimental tests to investigate the performance of extended blind-bolts were conducted, a holistic understanding of extended hollo-bolts remains to be at scarce because of certain limitations in the experimental program. In this work, the tensile pull-out behaviour of extended hollo-bolt, has been extensively investigated for its performance with CFST column connections. The study is conducted initially by validating numerical models with existing experimental works, and later by conducting extensive finite element parametric studies to predict and understand the influence of various connection components. It is observed that, not only the presence of concrete in the hollow steel tube has led to reduced deformation of the connection, but also the bolt embedment length into the concrete core has significantly improved the strength and stiffness. The study observes significant change in connection behaviour due to influence of change of parameter profiles. In this study, the various failure modes that can be altered as per combinations of the connection component strength are elaborately discussed.

Keywords

Hollo-bolts, blind-bolts, CFST, bolted connection, tensile pull-out, composite behaviour

1. Introduction

The widespread use of concrete filled steel tubes (CFST) have not only been popular owing to its superior strength, ductility, and aesthetics but also due to its better fire resistance, lesser vibration sensibility and ability to resist higher loads in post-yield capacity. An extensive research finding on CFSTs can be observed from the literature that includes its behaviour under compressive loading, eccentric tension, and seismic loading [1-5]. Further to this, the connections for closed sections like CFST with opens sections like I- or H-beams are generally observed to be welded [6], which involves heat affected zones and fabrication can be cumbersome which requires skilled manpower and thus expensive. These issues can be overcome by use of bolted connections which offers easier and faster fabrication, but its use has been limited due to severe slippage of bolts, column surface deformation and insufficient moment resisting capacity [7]. The use of bolts has also been highly preferred for fabrication in modular integrated constructions (MiC) which is gaining popularity due to its rapid construction and easy installation [8, 9]. Again, fabricating closed or box sections with standard bolts is not straight forward as one could not access the other side of the bolt and thus the "blind-bolt" was proposed to connect an open section with a closed section or hollow tube. Blind bolts can be inserted and tightened from one side of the tube without accessing the other end of the bolt inside the hollow tube and required clamping strength between the closed and open section could also be achieved. The hollo-bolt made by Lindapter International UK [10], the Oneside blind-bolt manufactured by Ajax Australia [11], the toggle blind-bolts manufactured by BlindBolt UK [12], and the slip-critical blind-bolt (SCBB) proposed by Wang *et al.* [13] are various forms of blind-bolts that has been used in connection fabrications for hollow or box sections with cavity.

Developing a rigid or semi-rigid moment-resisting bolted connection has always been a challenge for structural engineers. It is also worth mentioning that purely bolted connections have been explored to a lesser extent, and currently no guidelines are available for such connections [14]. In such a scenario, the blind-bolts have attained several modifications to enhance the connection performance suited for moment-resisting frames. Goldsworthy and Gardner [15] observed that if the studs or bolts can fully penetrate the concrete core in CFSTs it can help in increasing strength, stiffness and anchorage capacity of the connection. Later in the recent years blind-bolts have been modified to have an extended shank length that would not only provide higher strength and stiffness but will also be feasible for easy fabrication and avoid any brittle failure. The blind-bolts made by Ajax Australia was modified with an extended threaded shank fitted with a circular headed nut, called as the headed anchored blind bolt (HABB) by Yao *et al.*, [16] and also later investigated by Oktavianus *et al.* and Agheshlui *et al.* [17, 18] on single bolted CFST connection behavior. Group bolted connections under pull-out tests were also investigated using the HABB by the same research group [19, 20], and observed higher performance in terms of enhanced strength and stiffness as compared to standard blind-bolts. The hollo-bolt manufactured by Lindapter International (UK), which is another common form of blind-bolt was also modified with extended bolt shank and headed circular nut by Pitrakkos *et al.* [21] and named it as the extended hollo-bolt (EHB). The investigation with EHB indicated enhanced stiffness as compared to the standard hollo-bolts. The enhanced performance of EHB has been attributed to the concrete anchorage that helped in significantly reducing the deformation and slip of the bolt. The efficiency of group of EHB was also assessed and moment resisting connections with rigid or semirigid behavior could be achieved as observed by Tizani *et al.* [22]. Investigation on EHB connection in CFST column with varied slenderness and concrete type was also carried out by Tizani *et al.*[23], and observed that behavior can be influenced by column tube thickness and use of light weight concrete leads to reduced strength and stiffness, but the experiment was limited by use of single embedment length of the bolt in to the concrete core.

It is worth mentioning that the re-usable test setup used in the experiment [21] involved thick tube of 20 mm and possibly because of this all bolts have attained its ultimate strength and failed by bolt shank necking. It was also observed that the strength, stiffness, and ductility of EHB was not dependent on its embedded length into the concrete core. The findings also include that the grade of infill concrete in the box section had limited influence on the ultimate strength and global deformation of the connection. But, in a realistic EHB bolted connection, the global behavior may not be governed by the bolt strength and it is anticipated that a longer embedment length of the EHB will have significant influence. Also, the connection may not always fail by bolt necking but may also fail by other modes like concrete crushing or tube wall yielding of the CFST column. The connection behavior can also be influenced by grade of concrete due to its change in elastic modulus with the compressive strength. Thus, to further investigate the actual behaviour of an EHB bolted connection, this work will delve into a realistic approach. The work will also complement the existing bolt tensile pull-out findings as numerical studies of the EHB are very limited in the literature.

2. Methodology

To investigate the behaviour CFST bolted connection using EHB a systematic numerical approach has been adopted. Initially, an extensive finite element (FE) modelling was carried out to validate existing experimental tests in three stages: (a) numerical validation of hollow circular, square and octagonal stub column tests, (b) numerical validation of square CFST stub column tests, and (c) numerical validation of blind-bolted CFST connections under tensile pull-out loading. This will not only be helpful to carry out further extensive parametric studies but will also generate reliability of the numerical models. The experimental investigation by Zhu *et al*. [24] was adopted for validating the numerical models generated for hollow stub columns as shown in Table 1. For the validation models for square CFST stub column tests, experimental works conducted from various parts of the globe [25-29] were selected as presented in Table 2, and their FE models were generated based on available information. The notations used in Table 1 and Table 2 are listed here as: B is column width for square or octagonal tube, Dia is the column diameter for circular tube, t is tube thickness, L is column height, f_y is tube yield strength, f_u is tube ultimate tensile strength, E_s is steel tube elastic modulus, f'_c is cylinder compressive strength of concrete and E_c is concrete elastic modulus.

For the validation of tensile bolt pull- out tests, the experimental works were mostly based in Australia, Hong Kong, and the United Kingdom (UK), and were modelled to replicate the behaviour as observed during the testing program. The summary of test date for tensile bolt-pull out test is presented in detail in Table 3. The tests conducted in Australia by Yao *et al.* and Agheshlui *et al.* [16, 18] were based on HABB connections with CFST, the investigations caried out in Hong Kong by Xu *et al.* [30] were based on SCBB connections fitted with hollow octagonal tubes, and the test conducted in UK by Pitrakkos *et al.* [21] were based on EHB connections with concrete filled steel boxes. It is worth mentioning that the bolt components and the bolting mechanism of HABB, SCBB and the EHB are distinctive, and therefore requires careful modelling and arrangement of the connection system. In this current research program, HABB, SCBB and EHB were modelled to validate the numerical models using the existing experimental programs. A total of 14 stub column tests and 14 tensile pull-out tests of blind-bolted connections from the existing works have been used to validate the numerical models. Further to this, after ascertaining reliability of the FE models, the EHB model was adopted to conduct an extensive numerical parametric study and assess the connection behaviour with concrete filled steel tubes. The notations used in Table 3 are listed here as: *B* is column diameter or column width, *t* is steel tube thickness, *H* is column height, *D* is bolt diameter, f_y is tube or bolt yield strength, f_u is tube or bolt ultimate tensile strength, E_s is tube or bolt elastic modulus, f'_c is cylinder compressive strength of concrete, E_c is concrete elastic modulus, δ is steel contribution ratio, and ξ is confinement ratio.

3. FE modelling and validation

The numerical modelling program is initially adopted to generate accurate FE models by validating existing experimental models and then create further new FE models to undertake extensive numerical studies. For the purpose of numerical modelling the commercially available FE software ABAQUS [31] was used and as discussed above, the validation work was also carried out in 3 stages, FE validation of hollow stub columns, validation of CFST stub column tests and FE validation of bolt tensile pull-out tests. For replicating true experimental models using FE techniques all available material information along with all possible boundary conditions mentioned in the literature are extracted and applied. The following subsections discusses briefly about the modelling aspects and validation results.

3.1 Modelling aspects

In this work, for steel material modelling, the stress-strain behaviour model proposed by Yun and Gardner [32] was adopted which offers a multi-linear curve and is based on an extensive analysis of hot-rolled steel. It is expected that this steel material model will be suited for the advanced numerical simulations where gradual loss of stiffness is important. The predictive equations proposed in [32] were further used to obtain the true stress and true strain. The Young's modulus of elasticity E_s , for steel and bolt components was considered as 210 kN/mm^2 and Poisson's ratio as 0.3 in absence of experimental data.

For modelling the concrete core for all the validation models, the concrete damage plasticity (CDP) model was adopted as available in the FE software package. The CDP model not only provides with general capacity for predicting behaviour of quasi-brittle materials with a proper representation of inelastic behaviour but also can present the concrete crushing and tensile cracking damage. The CDP parameters such as the concrete dilation angle ψ was adopted to be 40° for square or rectangular sections, the eccentricity $\in$ is adopted as the default value of 0.1, K_c which is defined as the ratio of Mises equivalent stress on the tensile meridian on the compressive meridian is considered to be 2/3, and such a combination is observed to have best prediction for concrete filled steel rectangular tubes. To predict the confined concrete compressive behaviour the 3-stage model proposed by Tao *et al*. [33] has been adopted.

To further consider the influence of concrete crushing and concrete cracking the compressive and tensile damage parameters were also used in the CDP model which can be applied via the "suboptions" tool. For tensile damage, the bi-linear tension softening behaviour was obtained from tensile stress versus cracking displacement value, and where the area under the curve is considered as concrete fracture energy. The Young's modulus of concrete is assumed to be $4700\sqrt{f'_{cc}}$ as per ACI 318–08 in absence of experimental data and Poisson's ratio taken as 0.2. A representative confined concrete compressive and tensile softening behaviour is shown in Fig. 1. The elements used for modelling of column tubes were S4R which is four node reduced integration shell element. For all other components like concrete, bolt, and bolt components the solid element C3D8R which is a general-purpose linear brick element was used. The sizes of these elements were carefully selected to minimize its effect, and the smallest size used in these simulations was of 5 mm considered suitable for bolt and its components. The surface-to-surface interaction between concrete and steel tubes in CFST were provided with "penalty" friction formulation along with a "hard" contact behaviour. The interaction properties between bolt and bolt components with steel tube, steel stub and concrete also need to be carefully established to avoid any convergence issue which is very common for such a complex system which involves numerous contact surfaces comprising of different materials.

The extended hollo-bolt used in this study is high strength threaded bar which is simply an extension of the bolt shank fitted with a headed nut and consists of total 6 components as compared to 5 components in the standard hollo bolt. In practical application, the EHB installation through an oversized hole in the steel tube is simple which requires applying a wrench torque while holding the bolt steel washer. The bolt torque applied is dependent on the diameter of the bolt and the rubber washer present between the sleeve and steel washer helps in providing high clamping force. The bolt torque applied during in-situ installation, is replicated in numerical simulations by applying bolt pretension in the bolt shank region with the help of a reduced temperature load. The numerical model of the hollo-bolt is shown in Fig. 2. The modelling of hollo-bolt is simplified by combining the bolt shank, steel washer and the conical nut in a single part instance and the expandable sleeve as a separate part instance. For the extended hollo-bolt the bolt shank is simply extended to the desired length and a headed nut is included. The rubber washer is not included in the FE model as its purpose is to provide clamping force which will be replicated by applying a preload.

The boundary conditions as reported in the existing literature are also applied in the numerical models. To reduce the computational cost the models were generated as half or quarter models wherever possible and all required symmetry boundary conditions were applied. For the hollow and CFST stub column test, the bottom side had fixity end conditions and a displacement control compressive axial loading was applied in the free side and continued until the column section fails. Whereas, in case of bolted connection tensile tests, single bolted connections were applied with monotonic displacement control loading with a rate of 1 mm/min like most of the actual experimental loading rates. A representative image of FE models generated for corresponding experimental bolt pull-out tests in literature is shown in Fig. 3. The following subsection discusses about the results of the FE validation with the experimental counterpart.

3.2 FE validation

As previously discussed, the numerical validation has been carried out in three stages, initially for hollow steel stub columns under compressive loading, CFST stub column tests under compressive loading and then subsequently for bolt pull-out tests under tensile loading. Three important aspects, namely, the load deformation behaviour, ultimate load, and deformed shape of the hollow stub columns, CFST stub columns and bolt tensile pull-out tests are obtained using FE simulations and compared with their experimental counterpart.

3.2.1 Hollow stub column validation

The numerical validation for hollow stub columns are based on the works of Zhu *et al.* [24], which includes different geometry like square, circular and octagonal cross-sections. For the FE modelling of the hollow tubes the imperfection profile from buckling analysis of the lowest eigen value with an amplitude of certain fraction of tube wall thickness was considered. Amplitudes with fraction values of $t/10$, $t/50$, and $t/100$ were used to calibrate the performance of the stub models, and the imperfection model with $t/100$ was found to have accurate results and thus further used for modelling Though the use of $t/50$, and $t/10$ had no significant changes in the prediction of load capacity, but the softening behavior of the columns were affected specially of the circular columns. The numerical load-deformation behavior with the experimental counterpart is presented in Fig. 4 and a representative failure mode of the stub column is presented in Fig. 5. As observed from both the figures, the displacement behavior, peak load and the deformed shape of the FE models are in good agreement with the experimental observations.

3.2.2 CFST stub column validation

The FE validation results for CFST stub columns mentioned in Table 2 are presented here. The FE plots with the corresponding experimental load-deformation behaviour is presented in Fig. 6. For presenting a clear image, out of 11 square CFST stub column models considered for the validation, only 5 representative models are placed for comparison in Fig. 6. The ultimate load obtained by FE was also compared with the ultimate load obtained from laboratory experiment and code-based full plastic resistance N_{pl} for CFST stub columns and is presented in Table 4. The equation for N_{pl} by Eurocode 4 [34] is presented in Equation 1, where A_s is area of steel tube, f_{yd} is the design yield strength of the steel, A_c is cross-sectional area of concrete and f_{cd} is cylinder compressive strength of concrete. It is worth mentioning that for numerical modelling of CFST stub columns, the imperfection profile was neglected as due to the presence of concrete infill and confinement effect, the tube imperfection had little effect.

$$N_{pl} = A_s f_{yd} + A_c f_{cd} \tag{1}$$

As observed from the load-deformation behaviour in Fig. 6 and peak value comparison in Table 4, it can be stated that the FE models have attained good agreement with the experimental counterparts. The ultimate load had a maximum deviation of 6% when compared with experimental value and 8% when compared with value obtained by using Equation 1.

3.2.3 Bolt tensile pull-out validation

The bolt tensile pull-out tests as previously mentioned in Table 3 are used for the validation of FE models and are presented in this section. In this case, the tensile load versus bolt deformation behaviour, ultimate failure load and the bolted connection failure modes were generated using FE models and compared with the experimental test results. Though the current study is specifically based on hollo-bolt, the numerical validations of other bolts like the HABB and SCBB are also considered in addition to hollo-bolt (HB and EHB) as primarily there are very limited experimental tensile pull-out tests on hollo-bolts, and secondly, considering different types of bolts will also help to enhance the reliability of the numerical models for further study. Two representative images of comparison between numerical model and experimental observation are presented in Fig. 7 and Fig. 8, where the stages of hollo-bolt under tensile loading and concrete damage, respectively are shown. As seen in Fig. 7, when the bolt is tightened with the desired torque value, the bolt pretension is generated in the bolt shank, and subsequently as the loading increases the bolt expandable sleeve attains peak stress and ultimately fails when the loading is continued beyond the maximum capacity and these stages were well captured in the numerical model.

As reported by Pitrakkos *et al.* [21] the concrete infill in the loaded end of the CFST specimen with standard hollo-bolt involved a concrete breakout as shown in Fig. 8, which was due to the fastener slipping and the sleeves deforming leading to the concrete breakout. The failure modes during the experiment using HABB include concrete crushing failure, column tube wall yielding, bolt fracture, whereas, for the experiment using hollo-bolts the internal bolt fracture was the dominant failure mode for concrete filled specimens and expandable sleeve failure for hollow specimen. The comparison for numerical model and experimental results for tensile load versus bolt head displacement are presented in Fig. 9, where validations for connections using HABB bolts are presented in Fig. 9(a) - 9(i), connections using SCBB bolts are presented in Fig. 9(j) - 9(k) and connections using hollo-bolts are presented in Fig. 9(l) - 9(n).

As observed from Fig. 9, the bolted connection deformation behaviour obtained using FE models have a good agreement with their corresponding experimental counterparts. The important observations like, initial stiffness, yield loading point, ultimate load and the connection ductility all have a good match with the experiments. Table 5 presents a summary for the comparison of FE predicted and experimentally obtained ultimate load along with the observed FEA failure modes of the connection, which further confirms the proximity between the numerical models and experimental observations.

4. Numerical investigation and discussion

As observed from the previous sections, the FE models were generated having sufficiently good agreement with the experimental counterparts and therefore further extensive numerical investigation is carried out. In this section, a series of single hollo-bolted connection with CFST square column is considered for the study under monotonic tensile pull-out loading. Though the CFST columns under axial compressive loading can undergo full composite action with both steel and concrete contribution, but in a bolted connection under tensile loading the concrete contribution is very limited. In such a scenario, the standard hollo-bolt is developed as an extended hollo-bolt (EHB), in which the extended bolt shank with a headed nut will be used as an anchorage into the concrete core of the CFST column. This extended anchored bolt-shank is expected to introduce enhanced concrete contribution under tensile loading condition and thus an enhanced composite behaviour is attained by utilising strength of both steel tube and the infill concrete. Thus, to provide with a holistic understanding for EHB connections with CFST columns the influence of various parameters is very crucial in determining the connection behaviour. Parameters like presence of infill concrete, bolt embedment length, bolt grade, bolt diameter, concrete grade, tube thickness etc. are considered in the study and have been elaborately reported here. For the numerical investigation, initially a square hollow tube of regular dimension having cross-section 250 mm × 250 mm × 8 mm was considered, which can also be regarded as the control specimen, and can be classified as class 1-3 (stocky) cross-section as per [35]. The total length of the numerical specimen is adopted to be 1 meter. The steel tube is filled with concrete and the single hollo-bolt is fitted to the column via a rigid steel stub and is positioned at the centre of the column. The FE model and its cross-section components are presented in Fig. 10. The numerical specimens have been designated as a combination of its component properties, displayed as (1)-(2)-(3)-(4)-(5), where 1st component refers to bolt diameter in mm, the 2nd component as bolt grade, 3rd component refers to bolt embedment length in mm, 4^{th} refers to concrete compressive strength in N/mm^2 and the 5^{th} component corresponds to steel tube thickness in mm. While designing it needs to be checked that the length of bolt embedment should be limited such that bolt from the opposite direction of the column can also be inserted and sufficient space is available for concrete between the headed nuts of the bolt.

Initially the effect of presence of concrete infill in steel tube under pull-out test with standard hollo-bolt is presented. As seen from Fig.11, the presence of concrete has not only enhanced the strength and stiffness of the connection but has retained the connection ductility. The peak load achieved by the specimen without concrete (D20-G8.8-E0-C0-T8) is only 60% as compared to the model with concrete infilled tube. This can be described as, in the hollow specimen most of the tensile loading is carried by the tube wall which yields upon applying higher load and thus the specimen fails by tube wall yielding. On the other hand, the specimen with concrete infill D20-G8.8-E0-C40-T8 has displayed improved strength and stiffness as the concrete confined by the steel tube helps in delayed yielding of the tube walls in other three directions of the column and there by the tube face with the connection yields at a higher load. This is worth mentioning that, for a hollow tube connection with standard hollo-bolt under tensile loading, the possible failure mode would be by tube wall yielding and gradual pull-out of the bolt sleeve, followed by cracks in the sleeve under further loading.

After the influence of concrete infill under tensile pull-out loading is ascertained, the effect of bolt embedment length inside the concrete core is investigated. The EHB of M20 having grade 8.8 is considered in the study, for which various bolt embedment lengths such as 0, 3*D*, 4*D* and 4.5*D* are considered for comparison, where *D* is diameter of the bolt. It is worth mentioning that for the bolts with diameter 20 mm, a torque of 300 Nm was applied. The FE models of hollo-bolts with various embedment length is shown in Fig. 12. The comparison of effect of various bolt elongation length for the EHB connections under tensile loading is also presented in Fig. 13. The specimens with higher bolt embedment depth with concrete anchorage have displayed not only higher stiffness but also enhanced strength and delayed yielding as compared to D20-G8.8-E0-C40-T8 which showed limited improvement with concrete infill and 0 embedment. For every longer headed bolt shank that was embedded into the concrete core, the area of concrete anchorage also increased, and thus more enhanced concrete contribution was possible leading to higher strength and stiffness in the connection. It is to be noted that, the EHB with 0 embedment (usually referred as standard hollo-bolt) has a small shank length embedded in the concrete core, which by default appears after bolt clamping, but as there is not headed nut attached, it offers no concrete anchorage. The mises stresses generated in the hollo-bolts having different embedment length is presented in Fig. 14, where the stresses generated for the bolt embedment of 90 mm is highest leading to more effective utilisation of bolt strength and enhanced concrete contribution.

The bolt with M16 having bolt torque of 190 Nm, was also investigated for the influence of higher bolt embedment length into the concrete core, as shown in Fig. 15, which also shows a similar trend of considerably enhanced strength and stiffness. But for a bolt embedment depth of 80 mm and above, there is no change in connection global stiffness and also the strength remains almost same, indicating bolt embedment beyond 5*D* for M16 bolts is not significant. It is also to be noted that, for a bolt embedment depth of 80 mm, there was observed delayed concrete crushing as compared to specimen having bolt embedment of 90 mm. From the above observations, it can be stated that with sufficient elongation of the headed bolt shank into the concrete core not only the infilled concrete contribution is enhanced but also the bolt capacity is utilised based on the embedment length.

For the case of M20 EHB connections, as the tensile loading is applied in the connection, the load is initially borne by the concrete anchorage and as the concrete fails in crushing this load is transmitted to the steel tube by bearing via the bolt washer. It is observed that, after the concrete damage, the load suddenly drops but again the load increases gradually and is transferred to the steel tube, and ultimately the connection fails by tube face yielding. Whereas, for the case of M16 EHB, the specimen with 60 mm, 72 mm, 80 mm, and 90 mm embedment length has a similar trend, but with 80 mm length provides high strength and stiffness with delayed concrete crushing. Fig. 16 presents the comparison for concrete damage for specimens with standard hollo bolt (0 embedment) and specimen with full embedment (90 mm) for the models D16-G8.8-E0-C40-T8 and D16-G8.8-E90-C40-T8 respectively, which clearly portrays the enhanced concrete contribution in the tensile loading. Fig. 16 (b) also shows that the concrete is damaged by formation of a concrete cone that initiates from the bolt head due to anchorage and extends up to the steel tube wall. The behavior of the column tube wall is also significantly influenced by the EHB embedded into the concrete core. As presented in Fig. 17, the model D20-G8.8-E0-C0-T8, which has no infill concrete displayed localised deformation around bolt hole and tube wall bending, whereas the model D20-G8.8-E0-C40-T8 having infill concrete have reduced tube wall deformation but tube wall yielding is pronounced due to resistance offered by the concrete which is confined by the tube. For the FE model D20-G8.8-E90-C40-T8, that consists of 90mm bolt embedment in concrete core displays enhanced tube wall yielding and high corner stresses induced due to enhanced area of concrete pull-out and subsequent load transfer by tube wall bearing.

The enhanced concrete contribution which evolved due to the headed bolt embedment can be measured by conducting a test in the same setup by removing the expandable sleeve and the bolt washer, such that the total load is borne by the concrete anchorage, as presented in Fig. 18. The behaviour of standard hollo-bolt with CFST column can be considered as the steel tube wall bearing contribution. The headed nut fixed to the bolt shank is the component that initiates the concrete anchorage, and its absence from the EHB will tend to behave like the standard hollo-bolt without any embedment length, as shown in Fig. 19. A little enhancement in strength could be possibly due to friction component between the headless extended shank and the surrounding concrete. This little enhancement might also be observed in an experimental setup because of the bond strength arising from the threads of the bolt shank and the adjoining concrete.

To investigate the influence of bolt grade for the EHB tensile pull-out test, grade of 8.8 and 10.9 are considered as they are most used for structural connection applications. The comparison is presented in Fig. 20, which shows very little distinction between the two grades of bolt except a little delayed yielding in case of connection with grade 10.9 (D20-G10.9-E90-C40-T8). The behaviour observed here is identical, possibly because the infill concrete of compressive strength C40 is a weaker component as compared to both the high strength bolts, and as a result, the connection fails by concrete crushing much before any bolt shank yielding and gradually the load is transferred to the tube wall by sleeve bearing.

Thus, to assess the influence of EHB bolt grade, a higher-grade concrete of compressive strength C70 was considered and observed that the EHB with grade 8.8 has reached its ultimate strength and failed by bolt shank necking. Whereas the connection with EHB grade 10.9 has attained a higher strength and failed initially by concrete crushing and gradually transferred the load towards tube wall yielding, as shown in Fig. 21. This also signifies that a concrete grade of C40 is strong enough for a grade 8.8 EHB to achieve its ultimate capacity, but such a situation is not desirable in a realistic situation where the connection fails by bolt necking. Except connection behavior D20-G8.8-E90-C70-T8, a failure pattern as observed in case of connection with bolt grade 8.8 (D20-G8.8-E90-C40-T8) and bolt grade 10.9 (D20-G10.9-E90-C40-T8 and D20-G10.9-E90-C70-T8) could signify a reliable behaviour as after concrete crushing failure the load is redistributed to the tube wall by bolt bearing, and eventually fails without bolt necking. The bolt having grades 8.8 and 10.9 with C70 at failure are presented in Fig. 22.

The influence of EHB bolt diameter is also considered in the study and presented in Fig. 23. With similar bolt embedment length of 90 mm, bolt grade, concrete grade and tube wall thickness, the diameter of the EHB bolt is varied and the connection behaviour is studied. Bolts of M12, M16 and M20 were considered and compared with similar embedment length of 90 mm, where for M12 it corresponds to 7.5*D*, for M16 it corresponds to 5.6*D*, and for M20 it corresponds to 4.5*D*. As expected, the bolts of M16 and M12 had reduced stiffness and connection capacity. The EHB connection with M16 had twice and M20 had 2.5 times the connection strength as compared to EHB connection with M12. The connection with M12 fails by extended bolt shank failure within the concrete core possibly due to long embedment length that led to reduced stiffness, and then the load is transferred to the steel tube wall by bolt bearing and concrete crushing is not observed in this case. To overcome the bolt shank failure in M12 bolts, a reduced embedment length of 4.5*D* (54 mm) was adopted and displayed similar strength and stiffness behaviour without any shank fracture as compared to an embedment length of 7.5*D*. For M16 bolt, the failure mode is initially by concrete cone crushing and then tube wall yielding, without any necking of bolt shank. The behaviour of M16 and M20 bolt diameter in presence of high strength infill concrete is presented in Fig. 24 where the change in stiffness and connection capacity is significant but both the connection fails by bolt necking as the concrete component is of comparatively higher strength then the bolts.

The grade of concrete infill in the CFST columns is also considered in the numerical investigation for tensile bolt pull-out tests and their connection behaviour is presented here. The connection behaviour with M20 and M16 bolts having concrete infill of grade C40, C50, C60 and C70 are considered as presented in Fig. 25 and Fig. 26, respectively. As higher grade of concrete is accompanied by higher modulus of elasticity, there has also been enhancement in connection stiffness with increasing concrete strength, but this increase is not significant beyond concrete grade C50. The initial yield point of the models also differed with the grade of concrete, where for case with C40 and C50 the initial yield occurred at an early stage and ultimately failed by concrete crushing and tube wall yielding. Whereas, for models with higher grade concrete, the initial yield point was delayed and displayed little concrete damage and the connections failed by bolt shank necking. The concrete damage along with column face deformation for FE models with lower grade concrete and concrete damage with bolt necking for FE models with higher grade concrete is shown in Fig. 27.

As previously mentioned, the numerical investigations were conducted using column cross-section 250 mm × 250 mm × 8 mm with varied bolt embedment length, bolt diameter, bolt grade and concrete grade and their responses are presented. But the CFST column tube thickness is also an important component that influences the EHB connection behaviour. It is also worth mentioning that the column tube wall or column face in bending contributes to the rotational stiffness of a connection and yielding of the tube face is also regarded as failure mode and therefore it also requires attention. Now column tube wall of varied thickness is considered for FE analysis and their connection behaviour is presented in Fig. 28. As observed from the figure, the initial stiffness is similar in all three cases as the strength is initially determined by concrete anchorage. As soon as cracks are initiated in concrete the load is fully transferred to the tube and the strength and stiffness is based on tube thickness. The model with tube thickness of 6 mm, which refers to a *B/t* ratio of 41.6, fails by excessive tube wall deformation beyond yielding as the tube face forms a weaker component and the bolt capacity is unable to be used significantly. The models with tube thickness of 10 mm and 12 mm, which refers to *B/t* ratio of 25 and 20.8, respectively and can be classified as class 1 sections are observed to have a different failure mode. In these two cases, the failure is initiated by concrete core failure but then due to sufficiently thick tube wall the connection strength continues to increase.

To investigate the influence of cross-section dimension which is a similar concept of *B*/t as discussed above was also considered. In this case, the cross-section width of the models was varied keeping all other factors including tube thickness as constant. The EHB connection behaviour for this case is presented in Fig, 29, where three cross-sections of size (250 × 250) mm, (275 × 275) mm and (300 × 300) mm are considered. It is observed that the initial stiffness is not altered by cross-section dimension due to similar bolt diameter and concrete strength, but there is alteration in secant stiffness. The reason attributed for this change could be due to reduction in confinement ratio for the models with larger cross-section.

As for the installation of hollo-bolts, a hole of significantly large diameter is required to be made in the column tube, for example, M20 bolts requires 35 mm diameter hole, and therefore the possibility for use of a larger diameter headed nut was investigated as there is enough space for the nut to be inserted though the column hole. In this case, bolt nut diameters of 28 mm (1.4×*D*),30 mm (1.5×*D*), 32 mm (1.6×*D*) and 35 mm (1.75×*D*) were investigated and the EHB connection behaviour is illustrated in Fig. 30. As observed, there is no significant change in the initial stiffness of the connections and there is no notable alteration in ultimate capacity due increase of nut area. Therefore, a nut diameter of 28 mm should be sufficient to develop the concrete strut provided the infill concrete is of minimum C40 and any concrete crushing in the anchorage junction is avoided at lower load levels.

5. Conclusion

In this article the research work is aimed for a holistic undertanding of extended hollo-bolted CFST connections under monotonic tensile pull-out loading. The current work holds significance as there are very limited information on tensile behaviour of EHB with CFST columns that includes the behavior of all components in a connection. As in a bolted connection, the failure mode is influenced by indivdual or by a combination of these components it is therefore essential to undertand the behavior by replicating a realsistic condition. Also, there is very rare numerical modeling of EHB connections in the literature and this work is expected to supplement further information on this type of connection. This numerical study is based on exisiting constitutive material models and experiments. Further experimental investigation supplemented by FE models are required for single and group EHB bolted-CFST connections for establishing any design guidelines.

For conducting the investigation initially the numerical techniques adopted are discussed followed by generating FE models for validating exisiting experiemental findings. The validation work was carried out in 3 stages, firstly, validation of FE models for hollow stub column tests, secondly, validation of CFST stub column tests and, finally, FE validation of tensile pull-out tests of bolted connections. It was observed that a good aggreement between the FE models and the experimental results were obtained, which also signifies that accurate numerical models can be generated for such complex blind-bolted CFST conenction. Further, after attaining relaiblity for the FE models, an extensive numerical study was conducted for single hollo-bolted CFST connection, and the major findings are briefly summarized here:

(a) In a CFST bolted connection, the use of EHB can significantly influence the connection behavior by enhancing the concrete contribution which usually is very limited with use of standard hollo-bolts. In this study, maximum possible embedment depth for column with B/t ratio of 31.25 was 4.5D using M20 EHB that led to 2.5 times increase in connection strength as compared to an unanchored connection.

(b) The EHB connection failure mechanism where the concrete crushing is followed by column tube wall yielding may be regarded as preferred failure mode as this can ensure enahnced concrete contribution alongwith significant utilization of bolt ultimate nominal capacity.

(c) Comparing M16 and M20 bolts, and studying their failure mode, it is suggested to adopt maximum embedment length of 4.5*D* for M12 and M20 bolts, whereas 5*D* for M16 bolts to achieve full stiffness and avoiding internal bolt fracture with delayed concrete cone formation.

(d) The study suggests a concrete grade of C40-C50 to be used as infill concrete as there is negligible improvement in connection stiffness beyond C50. Connection failure by bolt shank necking is observed with higher grade concrete of C70, but usually such a failure would not be expected in a realistic situation.

(e) As observed within the studied *B/t* range of 20.8 to 41.6, the connection stiffness is influenced mostly by *B/t* ratio for standard hollo-bolt connections. Whereas, for EHB connections, the stiffness is influenced by *B/t* ratio, concrete strength, bolt diameter and embedment depth.

(f) Though the headed nut plays vital role for developing the concrete anchorage, increasing the diameter from 28 mm (for M20 bolts) to beyond has no significant influence suggesting the available nut diameter is sufficient.

(g) The generated numerical models of the assembled EHB-CFST connection will be useful in identifying the capacity with regard to analysis of each component contribution.

Acknowledgement

The authors sincerely acknowledge the support from the Innovation and Technology Fund - Nano and Advanced Materials Institute (ITF-NAMI) for the project “Hong Kong Modular Integrated Construction (MiC) Innovations“ (PolyU/ ZS12) and from the Chinese National Engineering Research Centre for Steel Construction (Hong Kong Branch) at The Hong Kong Polytechnic University.

References

[1] W. Li, L.-H. Han, T.-M. Chan, Performance of Concrete-Filled Steel Tubes subjected to Eccentric Tension, Journal of Structural Engineering 141(12) (2015) 04015049.

[2] J.-Y. Zhu, T.-M. Chan, Behaviour of polygonal-shaped steel-tube columns filled with high-strength concrete, Proceedings of the Institution of Civil Engineers - Structures and Buildings 171(2) (2018) 96-112.
[3] L.-H. Han, W. Li, Seismic performance of CFST column to steel beam joint with RC slab: Experiments, Journal of Constructional Steel Research 66(11) (2010) 1374-1386.
[4] H.-S. Hu, Y. Liu, B.-T. Zhuo, Z.-X. Guo, B.M. Shahrooz, Axial Compressive Behavior of Square CFST Columns through Direct Measurement of Load Components, Journal of Structural Engineering 144(11) (2018).
[5] M. Abramski, Load-carrying capacity of axially loaded concrete-filled steel tubular columns made of thin tubes, Archives of Civil and Mechanical Engineering 18(3) (2018) 902-913.
[6] M. Zeinizadeh Jeddi, N.H. Ramli Sulong, M.M. Arabnejad Khanouki, Seismic performance of a new through rib stiffener beam connection to concrete-filled steel tubular columns: An experimental study, Engineering Structures 131 (2017) 477-491.
[7] M.Z. Jeddi, N.H.R. Sulong, Pull-out performance of a novel anchor blind bolt (TubeBolt) for beam to concrete-filled tubular (CFT) column bolted connections, Thin-Walled Structures 124 (2018) 402-414.
[8] A.W. Lacey, W. Chen, H. Hao, K. Bi, Review of bolted inter-module connections in modular steel buildings, Journal of Building Engineering 23 (2019) 207-219.
[9] E.-F. Deng, L. Zong, Y. Ding, X.-M. Dai, N. Lou, Y. Chen, Monotonic and cyclic response of bolted connections with welded cover plate for modular steel construction, Engineering Structures 167 (2018) 407-419.
[10] The Original Expansion Bolt for Structural Steel, in: L. International (Ed.) Bradford, England, 2013.
[11] ONESIDE Brochure B-N012 Data Sheet, AJAX Engineered Fasteners Victoria, Australia, 2002.
[12] Blind Bolt Technical Data, in: B. International (Ed.) Worcester, United Kingdom, 2020.
[13] W. Wang, M. Li, Y. Chen, X. Jian, Cyclic behavior of endplate connections to tubular columns with novel slip-critical blind bolts, Engineering Structures 148 (2017) 949-962.
[14] Y. Oktavianus, H. Goldsworthy, E.F. Gad, Behaviour of Headed Anchor Blind Bolts Embedded in Concrete Filled Circular Hollow Section Column, Australian Earthquake Engineering Society 2014 Conference, Lorne, Victoria, 2014.
[15] H. Goldsworthy, A. Gardner, Feasibility study for blind-bolted connections to concrete-filled circular steel tubular columns, Structural Engineering and Mechanics 24(4) (2006) 463-478.
[16] Y.H. Yao, G. Helen, G. Emad, F. Saman, Experimental Study on Modified Blind Bolts Anchored in Concrete-filled Steel Tubular Columns, Australian Earthquake Engineering Society, South Australia, 2011.
[17] Y. Oktavianus, H. Yao, H.M. Goldsworthy, E.F. Gad, Pull-out behaviour of blind bolts from concrete-filled tubes, Proceedings of the Institution of Civil Engineers - Structures and Buildings 168(10) (2015) 747-759.
[18] H. Agheshlui, H. Goldsworthy, E. Gad, S. Fernando, Tensile behaviour of anchored blind bolts in concrete filled square hollow sections, Materials and Structures 49(4) (2016) 1511-1525.
[19] H. Agheshlui, H. Goldsworthy, E. Gad, H. Yao, Tensile Behavior of Groups of Anchored Blind Bolts within Concrete-Filled Steel Square Hollow Sections, Journal of Structural Engineering 142(2) (2016) 04015125.
[20] Y. Oktavianus, H.M. Goldsworthy, E. Gad, Group Behavior of Double-Headed Anchored Blind Bolts within Concrete-Filled Circular Hollow Sections under Cyclic Loading, Journal of Structural Engineering 143(10) (2017).
[21] T. Pitrakkos, W. Tizani, Experimental behaviour of a novel anchored blind-bolt in tension, Engineering Structures 49 (2013) 905-919.
[22] W. Tizani, T. Pitrakkos, Performance of T-Stub to CFT Joints Using Blind Bolts with Headed Anchors, Journal of Structural Engineering 141(10) (2015) 04015001.

[23] W. Tizani, M. Mahmood, D. Bournas, Effect of Concrete Infill and Slenderness on Column-Face Component in Anchored Blind-Bolt Connections, Journal of Structural Engineering 146(4) (2020) 04020041.
[24] J.-Y. Zhu, T.-M. Chan, B. Young, Cross-sectional capacity of octagonal tubular steel stub columns under uniaxial compression, Engineering Structures 184 (2019) 480-494.
[25] C.S. Huang, Y.-K. Yeh, G.-Y. Liu, H.-T. Hu, K.C. Tsai, Y.T. Weng, S.H. Wang, M.-H. Wu, Axial Load Behavior of Stiffened Concrete-Filled Steel Columns, Journal of Structural Engineering 128(9) (2002) 1222-1230.
[26] S.P. Schneider, Axially Loaded Concrete-Filled Steel Tubes, Journal of Structural Engineering 124(10) (1998) 1125-1138.
[27] L. Guo, S. Zhang, W.-J. Kim, G. Ranzi, Behavior of square hollow steel tubes and steel tubes filled with concrete, Thin-Walled Structures 45(12) (2007) 961-973.
[28] K. Sakino, H. Nakahara, S. Morino, I. Nishiyama, Behavior of Centrally Loaded Concrete-Filled Steel-Tube Short Columns, Journal of Structural Engineering 130(2) (2004) 180-188.
[29] L.-H. Han, X.-L. Zhao, Z. Tao, Tests and mechanics model for concrete-filled SHS stub columns, columns and beam-columns, Steel and Composite Structures 1(1) (2001) 51-74.
[30] F. Xu, T.-M. Chan, Structural Behaviour of Blind-Bolted T-stub to Octagonal Tube Connections Using Normal and High Strength Steels, Ninth International Conference on Advances in Steel Structures (ICASS), Hong Kong, 2018, pp. 1510-1520.
[31] ABAQUS, Dassault Systems, Waltham, MA, USA, 2019.
[32] X. Yun, L. Gardner, Stress-strain curves for hot-rolled steels, Journal of Constructional Steel Research 133 (2017) 36-46.
[33] Z. Tao, Z.-B. Wang, Q. Yu, Finite element modelling of concrete-filled steel stub columns under axial compression, Journal of Constructional Steel Research 89 (2013) 121-131.
[34] CEN 1994-1-1, Eurocode 4: Design of Composite Steel and Concrete Structures – Part 1-1: General Rules and Rules for Buildings, 2009.
[35] EN 1993-1-1 (2005): Eurocode 3: Design of steel structures - Part 1-1: General rules and rules for buildings, 2005.

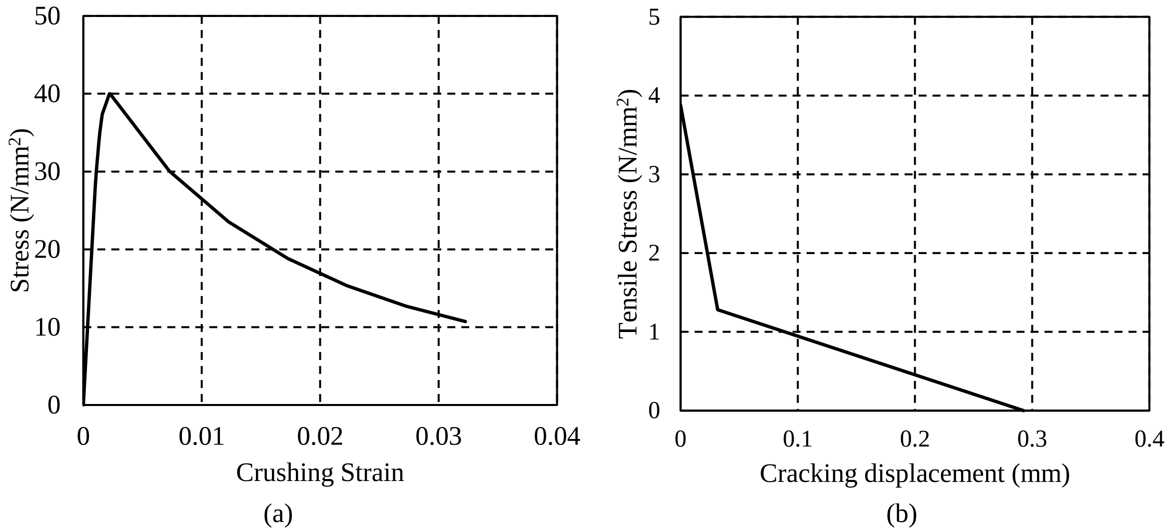

Fig. 1. (a) Concrete compressive stress-strain curve (b) Concrete tensile softening model.

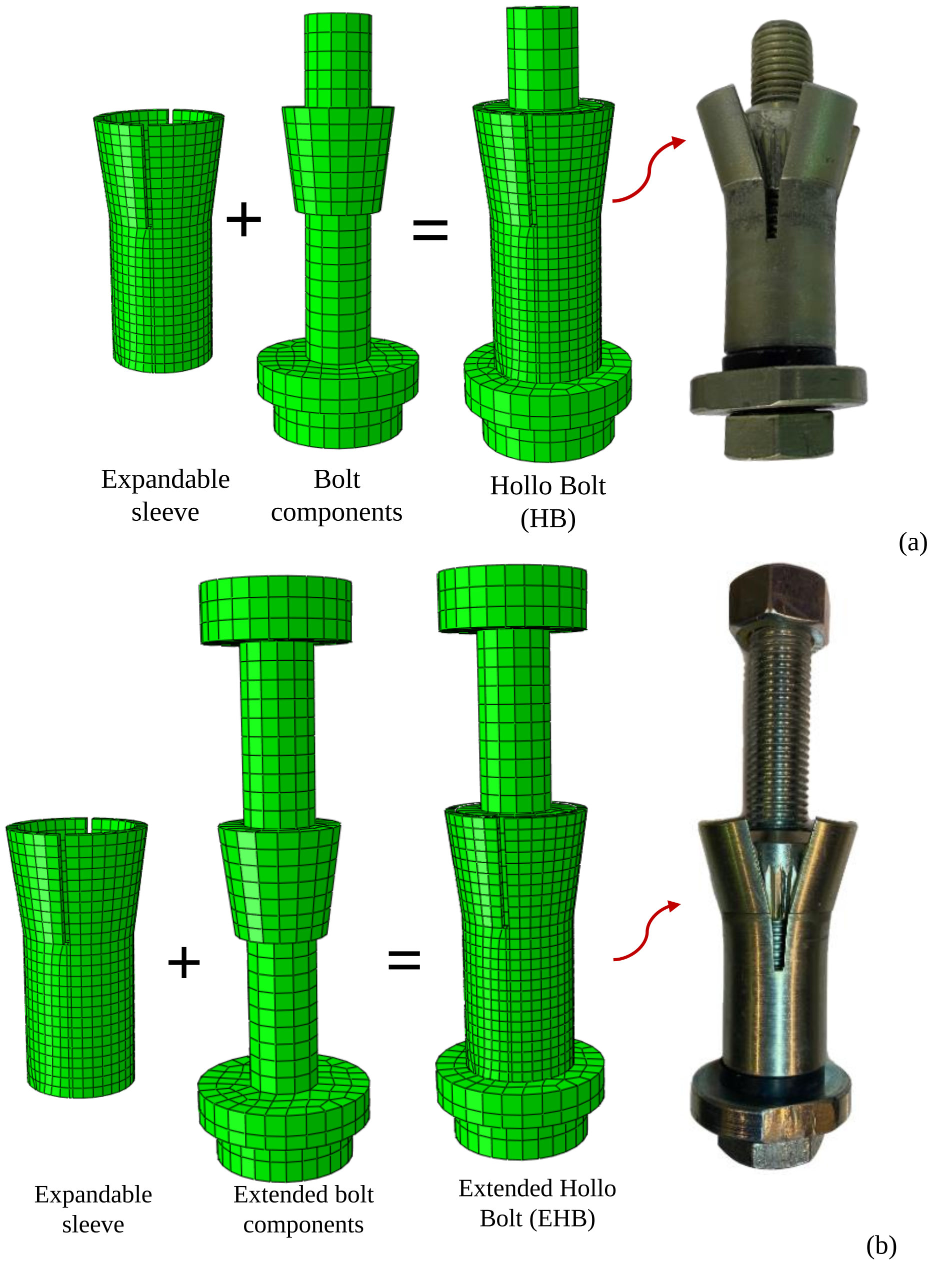

Fig. 2. FE model of tightened (a) standard hollo-bolt, and (b) extended hollo-bolt (EHB).

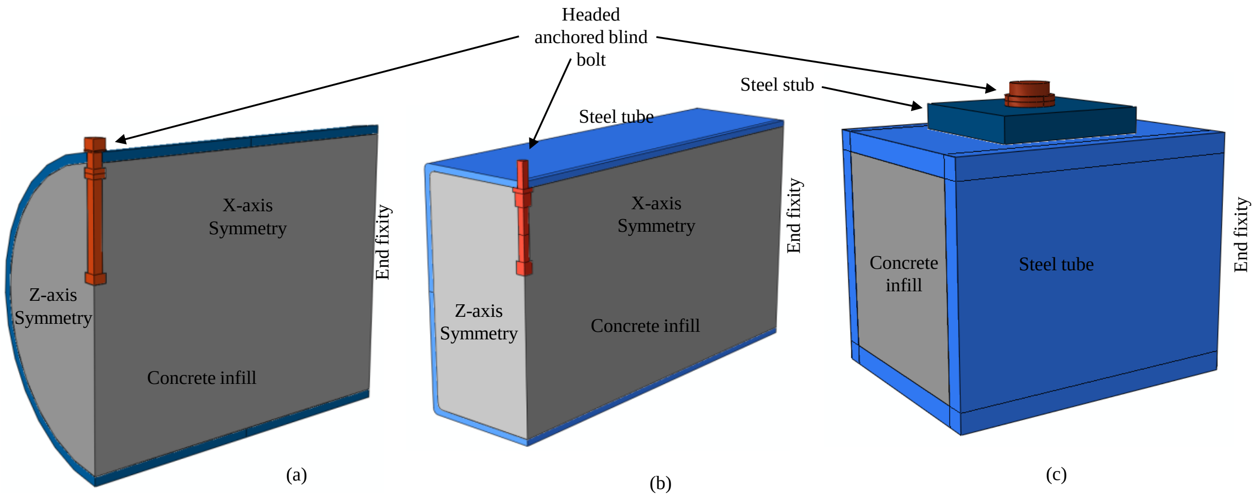

Fig. 3. (a) FE quarter model for test by Yao *et al.* [16], (b) FE quarter model for test by Agheshlui *et al.*[18] and (c) FE full model for test by Pitrakkos *et al.* [21].

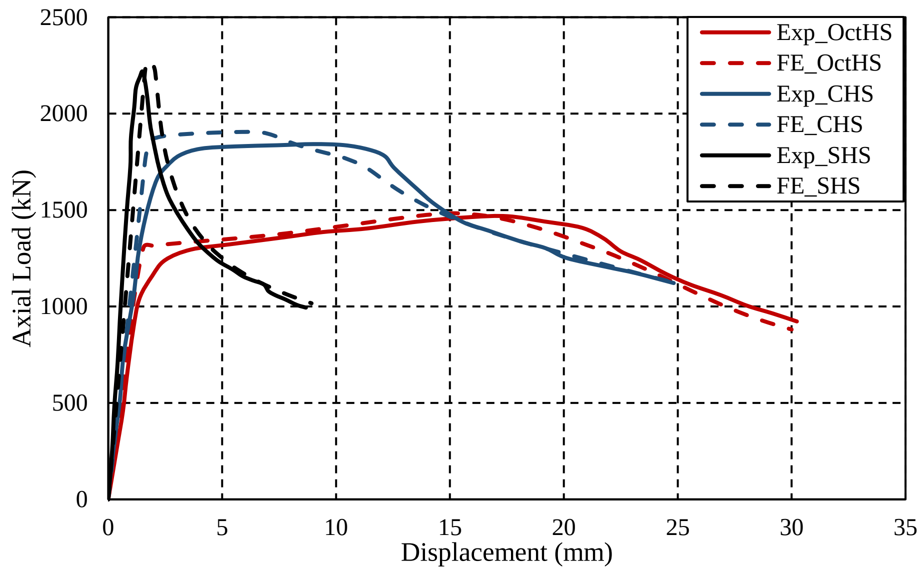

Fig. 4. FE validation of square hollow stub columns.

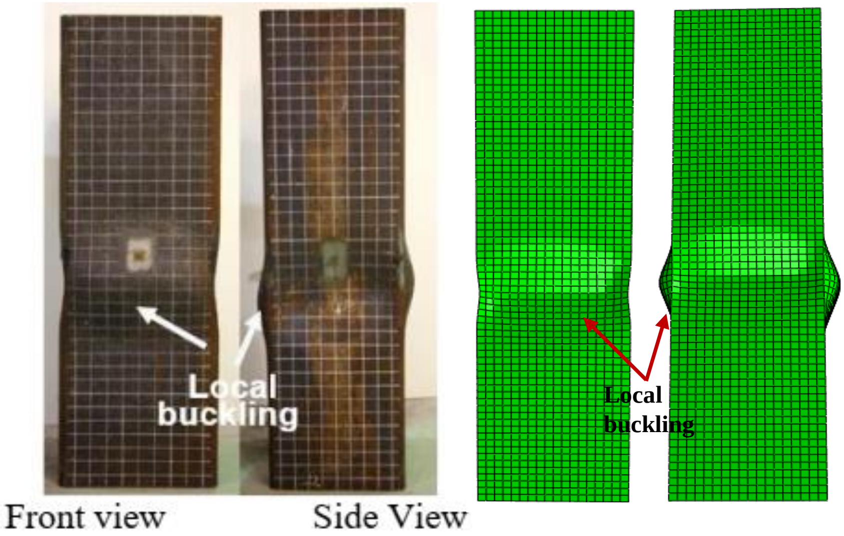

Fig. 5. Comparison of experimental [24] and FE for square hollow stub tubes.

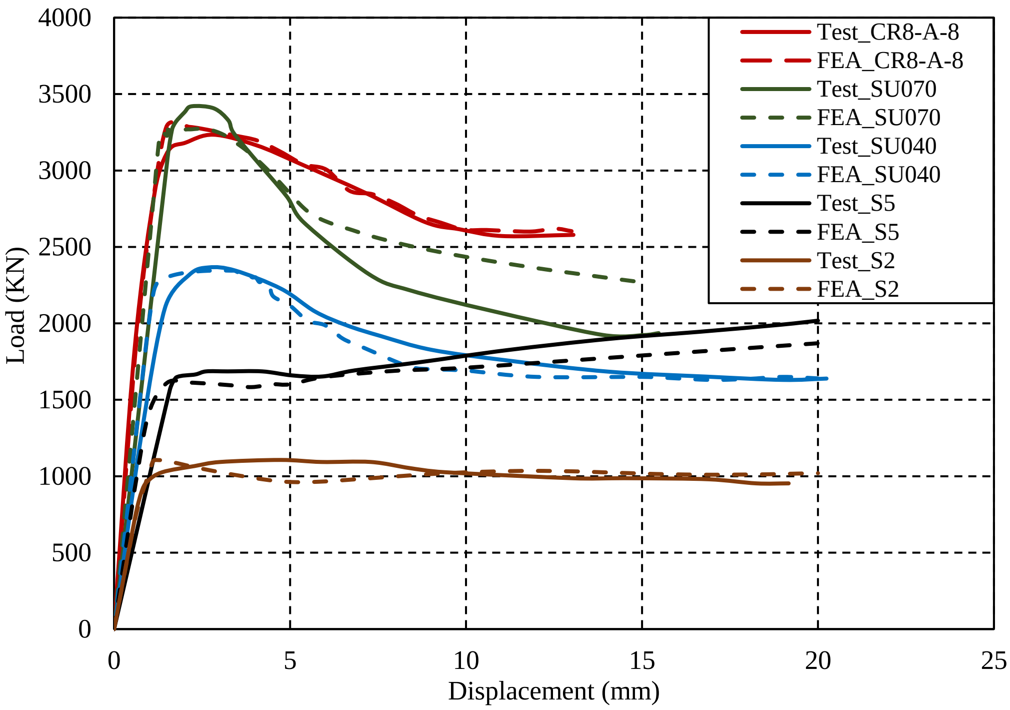

Fig. 6. FE validation of square CFST stub columns.

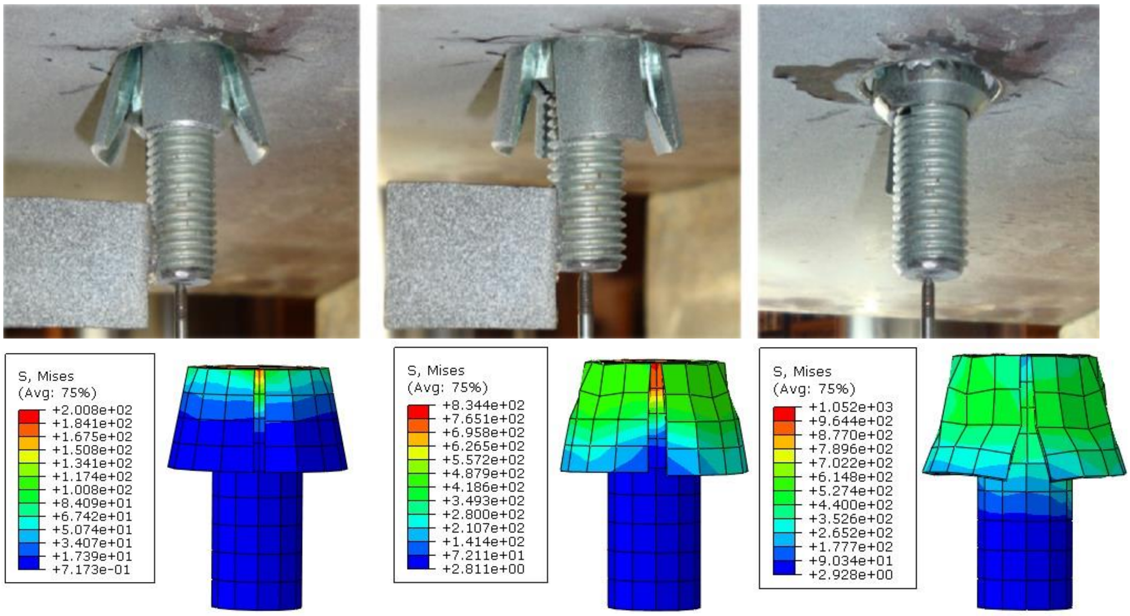

(a) at tightening (b) prior ultimate load (c) at failure

Fig. 7. Comparison of experimental [21] and FE for pull-out test of hollo-bolt.

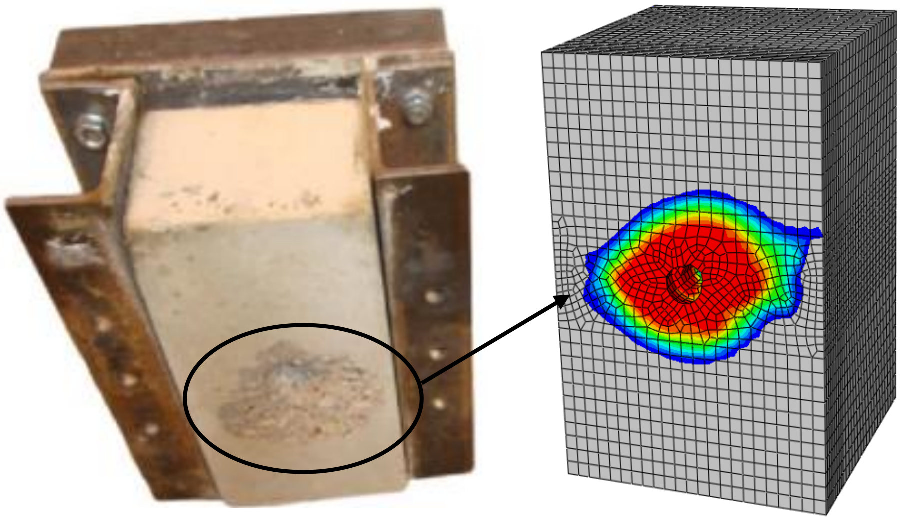

Fig. 8. Comparison of experimental [21] and FE for concrete damage with hollo-bolt.

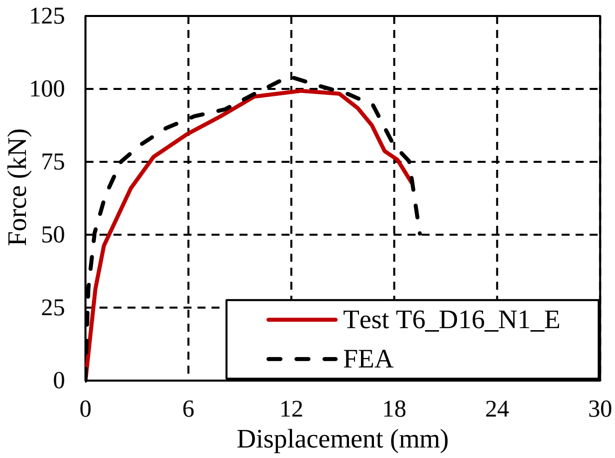
125
100
75
50
25
0
Force (kN)
0
6
12
18
24
30
Displacement (mm)
Test T6_D16_N1_E
FEA

(a)

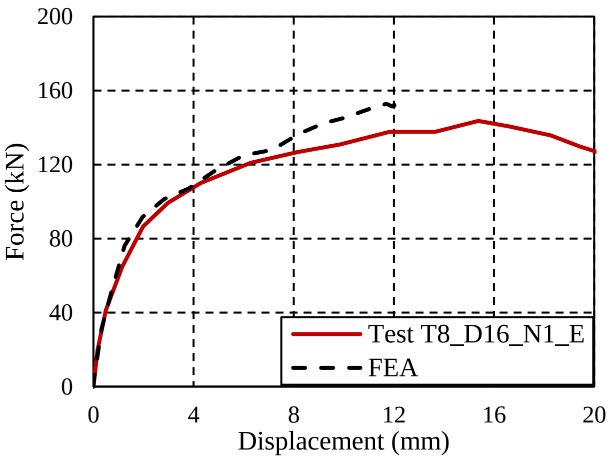
200
160
120
80
40
0
Force (kN)
0
4
8
12
16
20
Displacement (mm)
Test T8_D16_N1_E
FEA

(b)

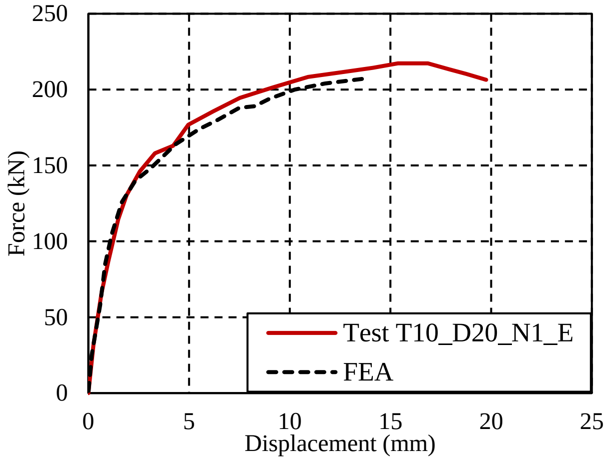
250
200
150
100
50
0
Force (kN)
0
5
10
15
20
25
Displacement (mm)
Test T10_D20_N1_E
FEA

(c)

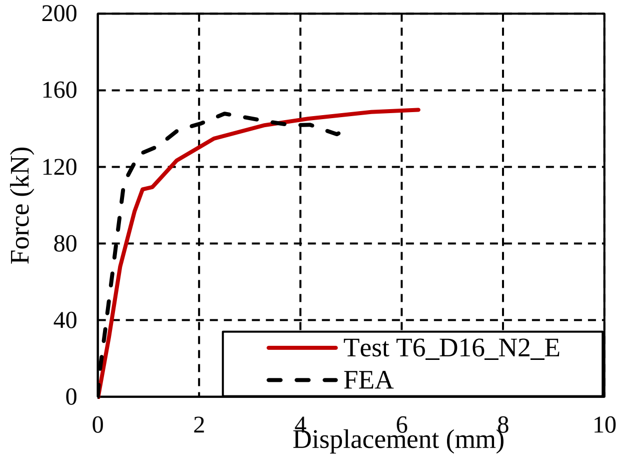
200
160
120
80
40
0
Force (kN)
0
2
4
6
8
10
Displacement (mm)
Test T6_D16_N2_E
FEA

(d)

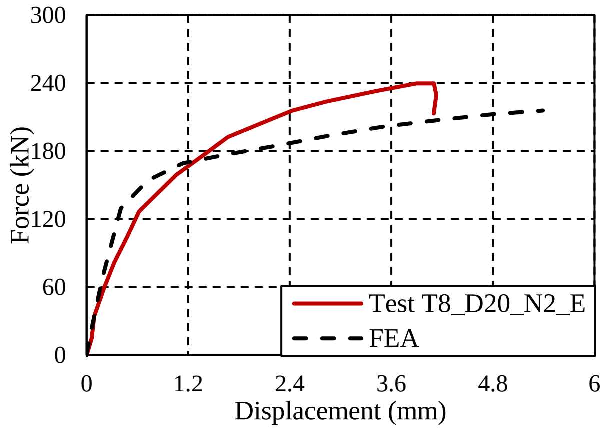
300
240
180
120
60
0
Force (kN)
0
1.2
2.4
3.6
4.8
6
Displacement (mm)
Test T8_D20_N2_E
FEA

(e)

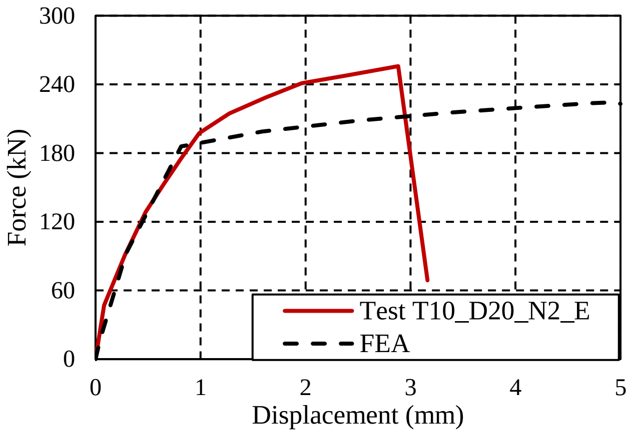
300
240
180
120
60
0
Force (kN)
0
1
2
3
4
5
Displacement (mm)
Test T10_D20_N2_E
FEA

(f)

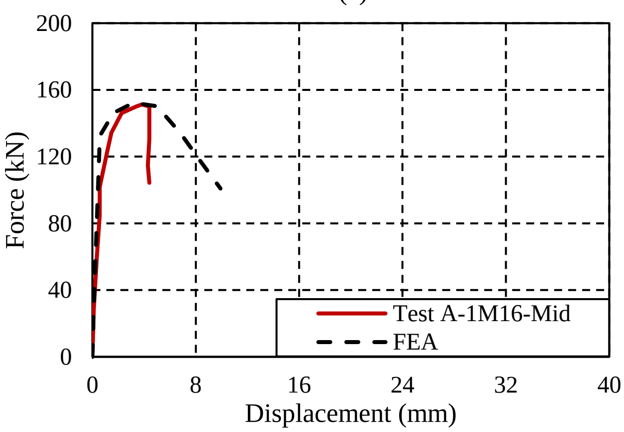
200
160
120
80
40
0
Force (kN)
0
8
16
24
32
40
Displacement (mm)
Test A-1M16-Mid
FEA

(g)

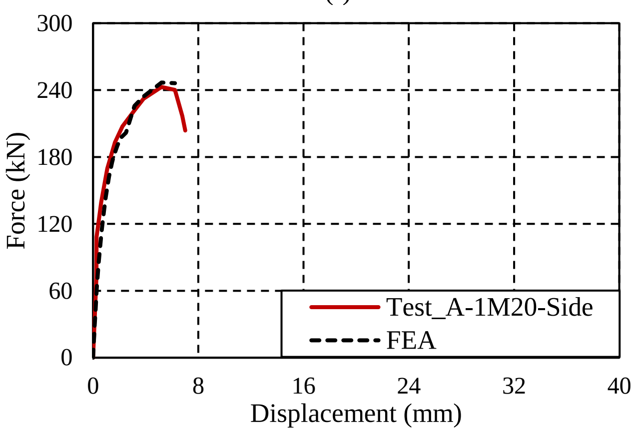
300
240
180
120
60
0
Force (kN)
0
8
16
24
32
40
Displacement (mm)
Test_A-1M20-Side
FEA

(h)

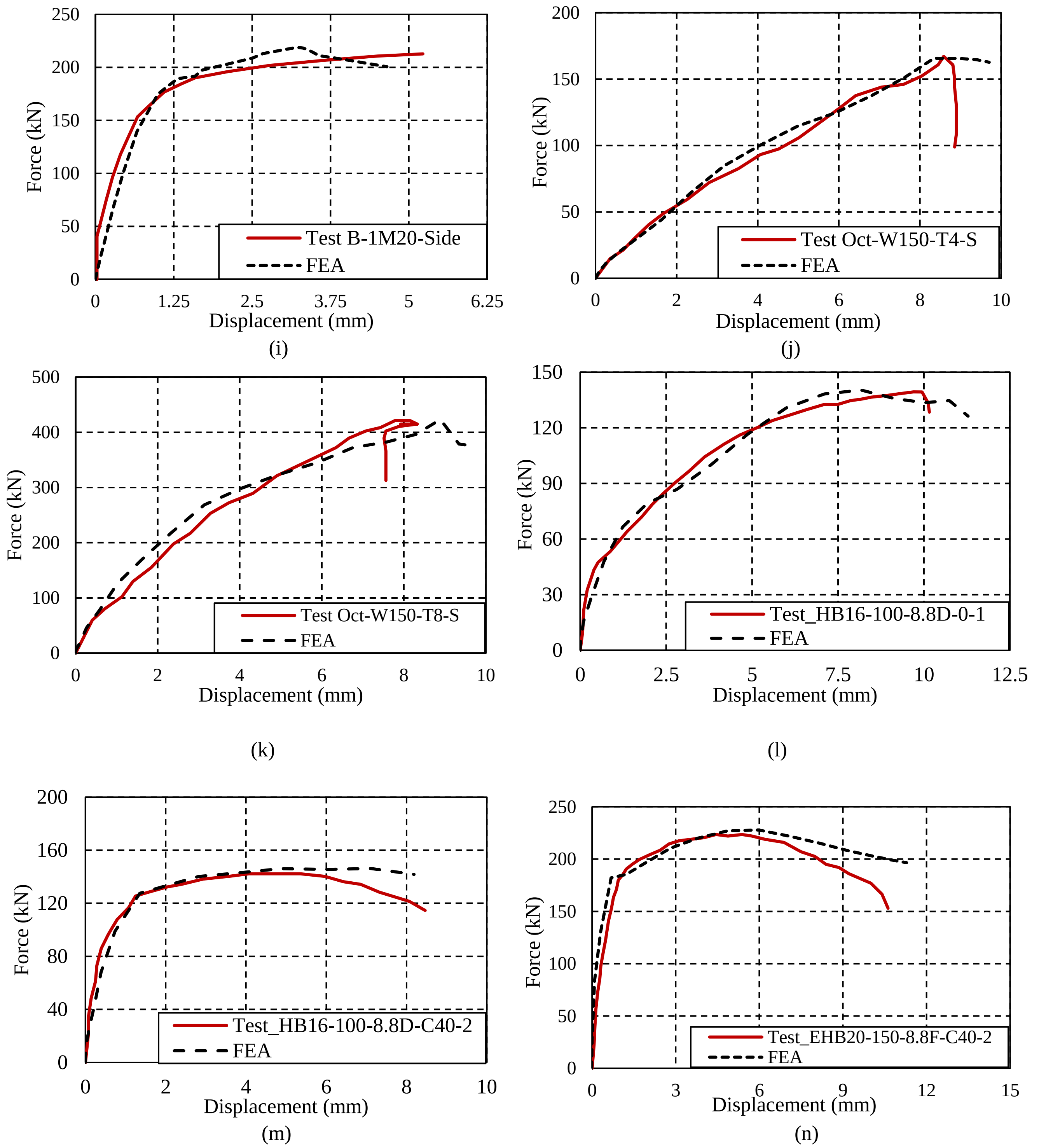

Fig. 9. FE validation of bolt tensile pull-out tests.

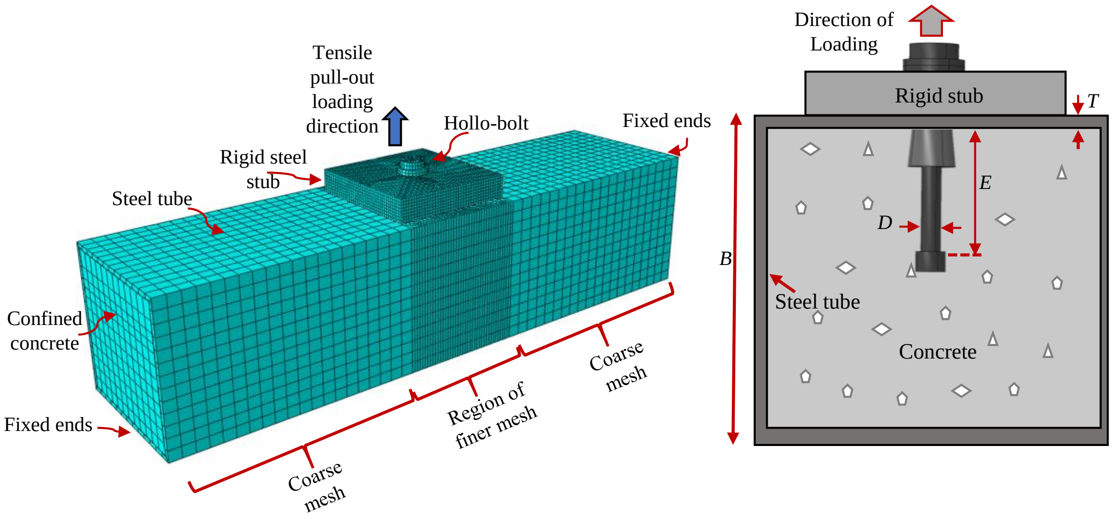

Fig. 10. FE model of the single hollo-bolted connection and cross-section components.

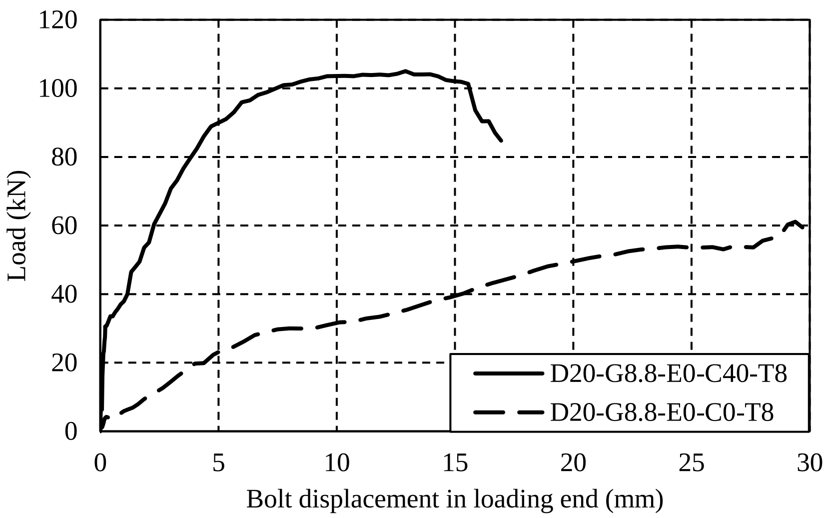

Fig. 11. Comparison of specimens with and without concrete in tube.

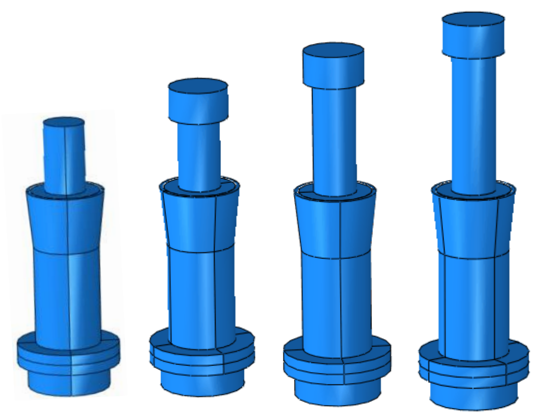

Fig. 12. FE models of hollo-bolts with various embedment lengths.

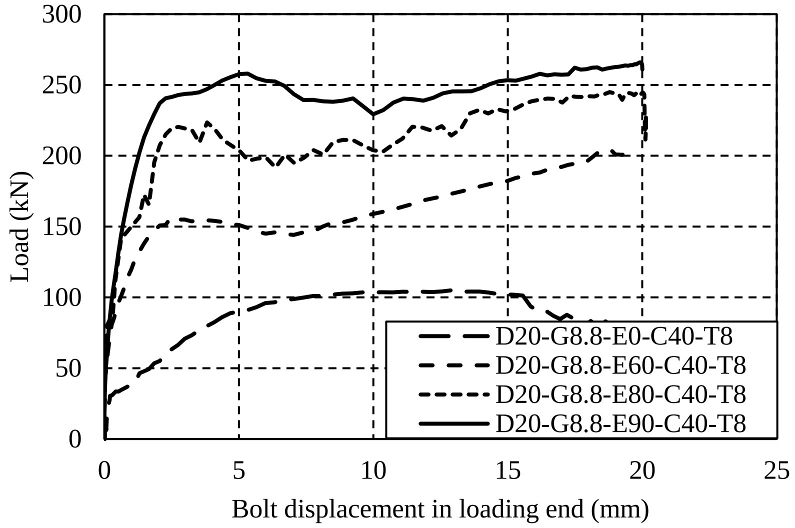

Fig. 13. Behaviour of M20 EHB connections with various embedment lengths.

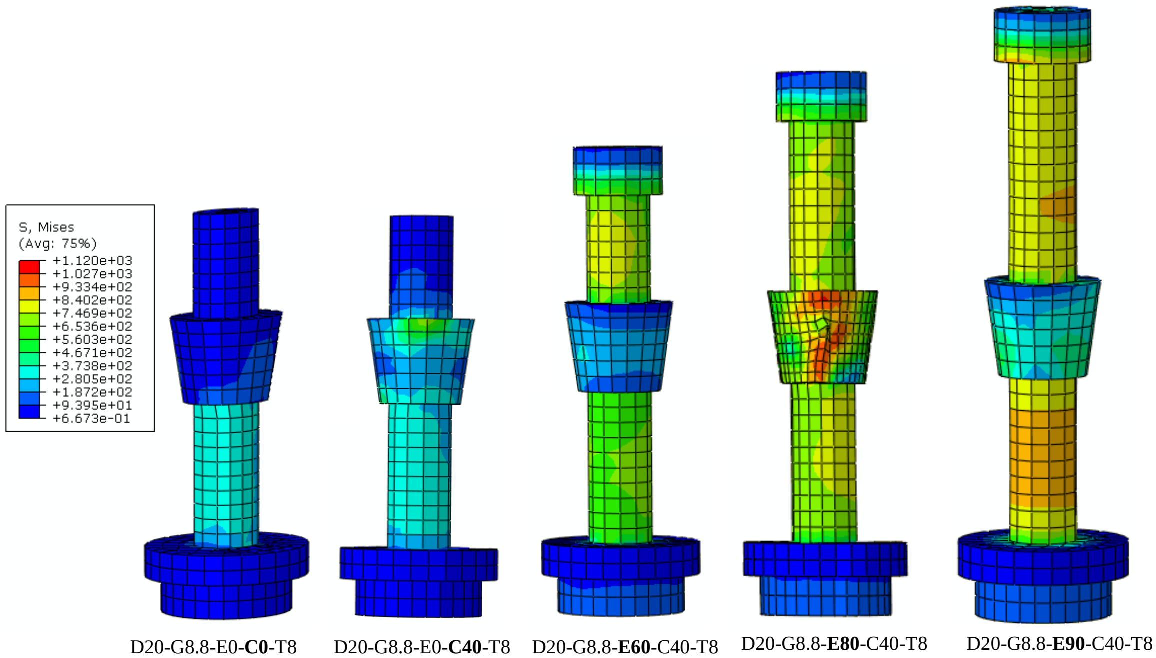

Fig. 14. Mises stresses in bolt shank with various bolt embedment length in concrete.

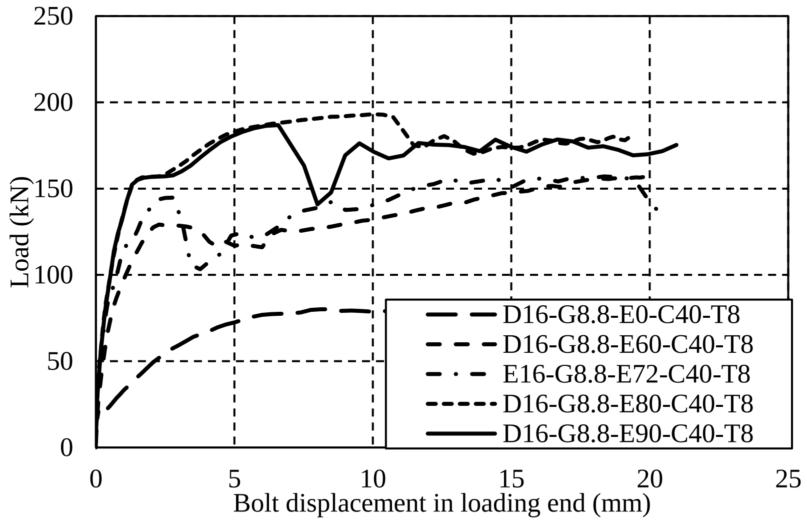

Fig. 15. Behaviour of M16 EHB connections with various embedment lengths.

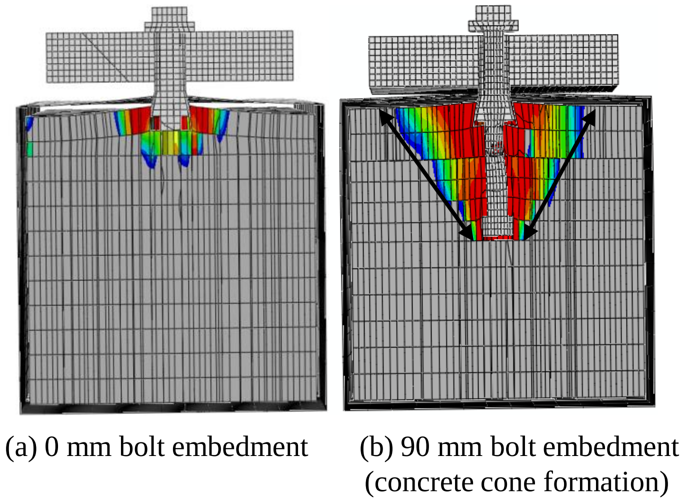

Fig. 16. Concrete core damage for M16 bolts with no embedment and full embedment.

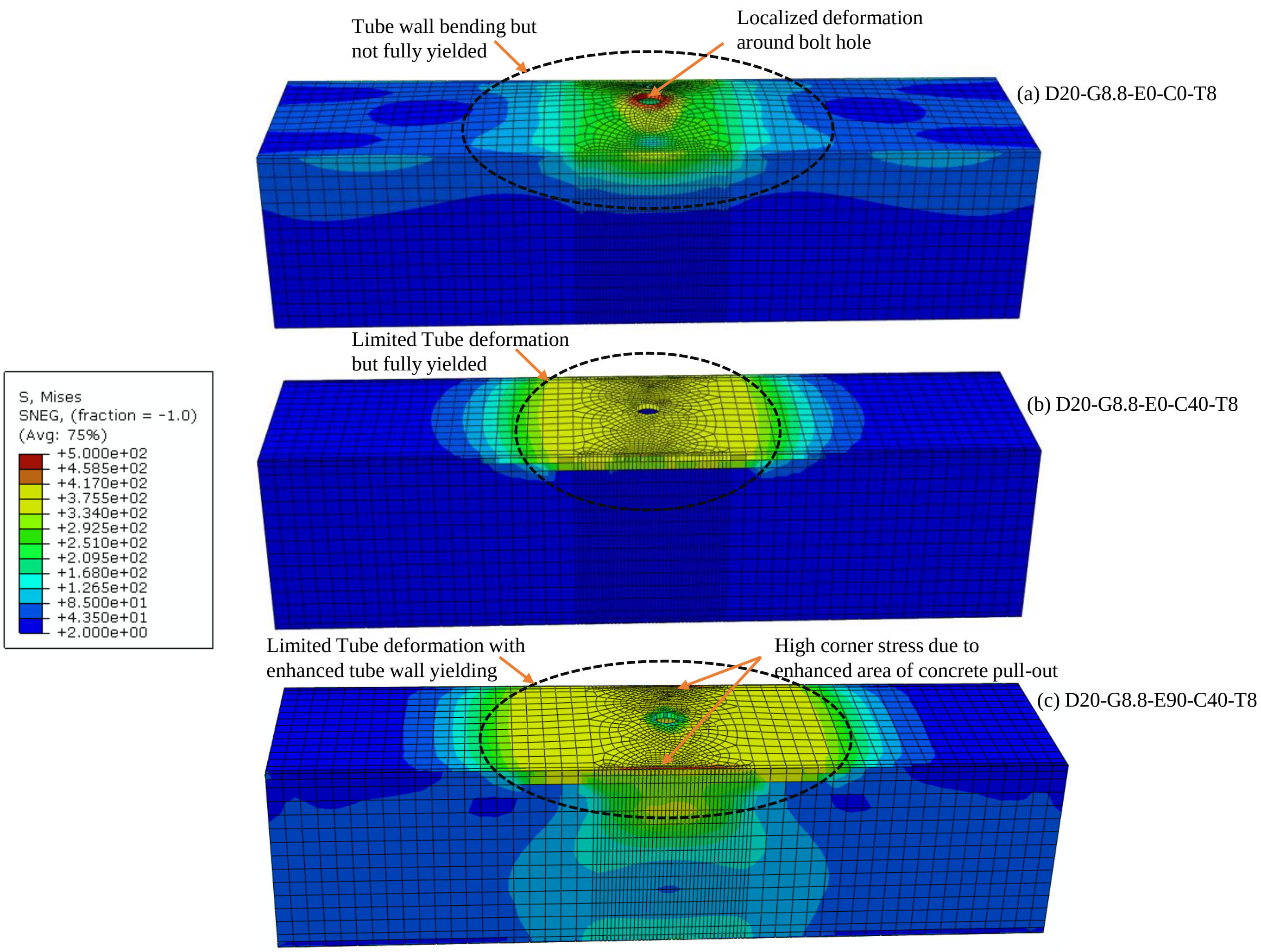

Fig. 17. Stress distribution in tube (a) without concrete (b) with concrete and 0mm bolt embedment (c) with concrete and 90mm bolt embedment depth.

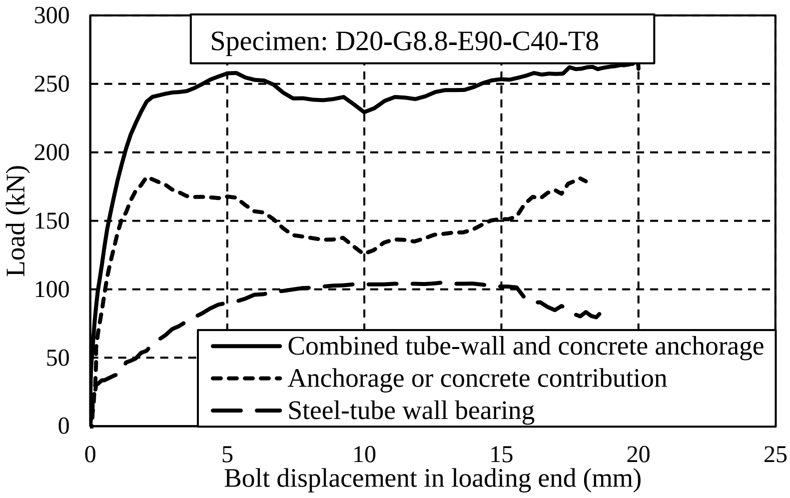

Fig. 18. Concrete and steel tube contribution in tensile loading

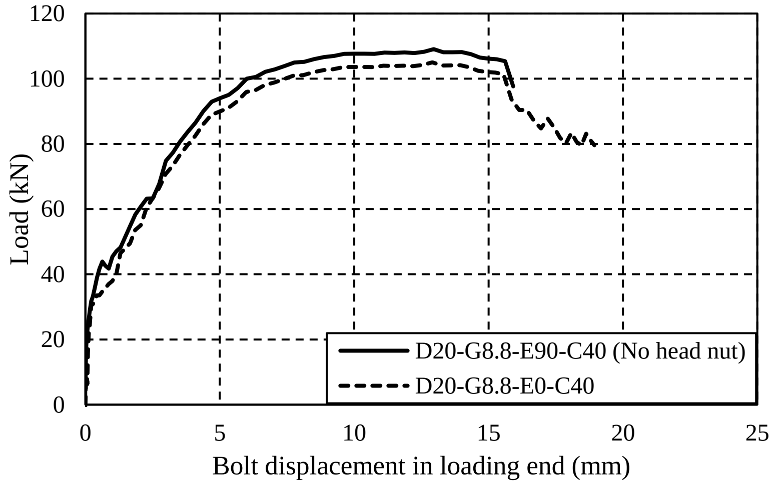

Fig. 19. Behaviour of EHB without nut and standard hollo-bolt.

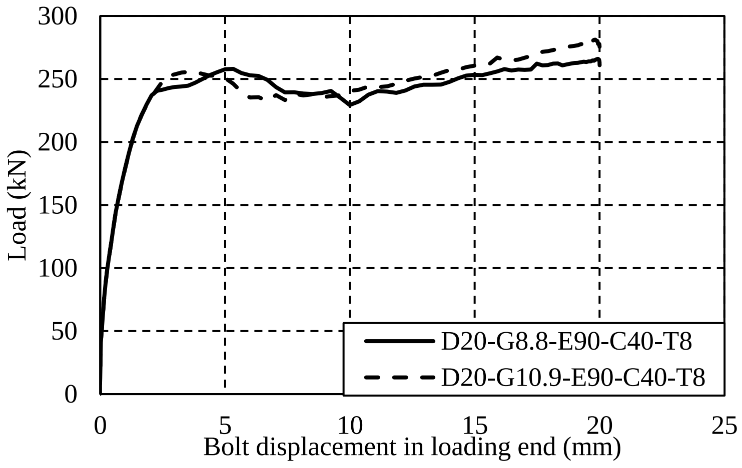

Fig. 20. Behaviour of EHB connection with bolt grade 8.8 and 10.9 with concrete C40.

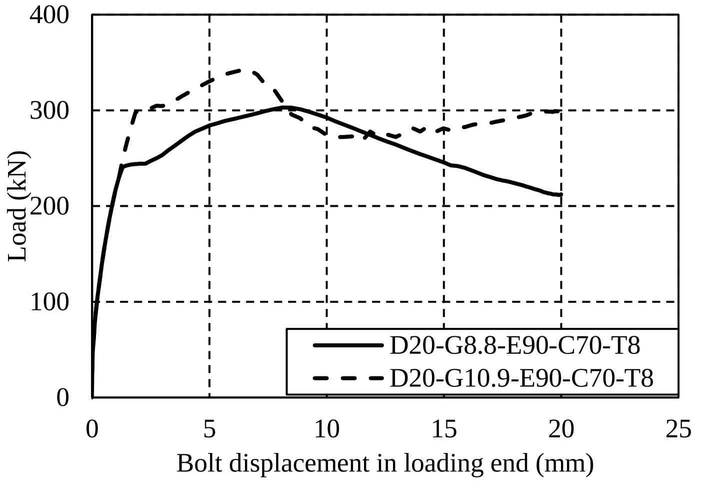

Fig. 21. Behaviour of EHB connection with bolt grade 8.8 and 10.9 with concrete C70.

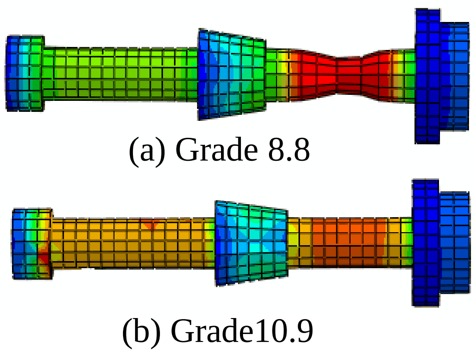

Fig. 22. Bolts at failure with concrete grade C70.

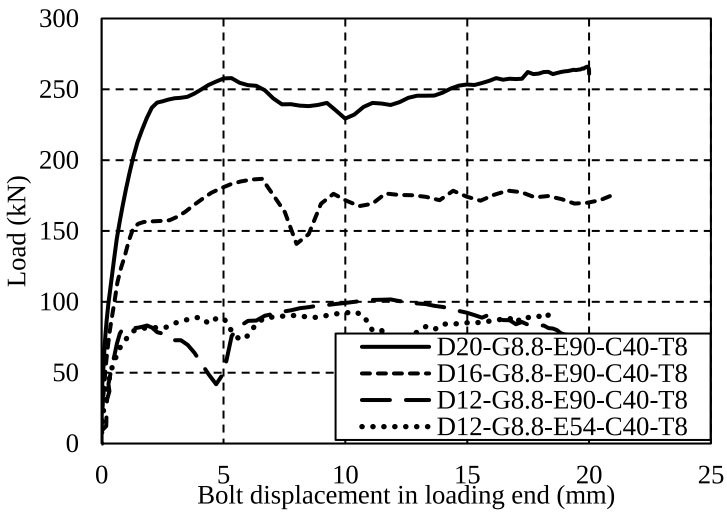

Fig. 23. Influence of bolt diameter in EHB connections with C40.

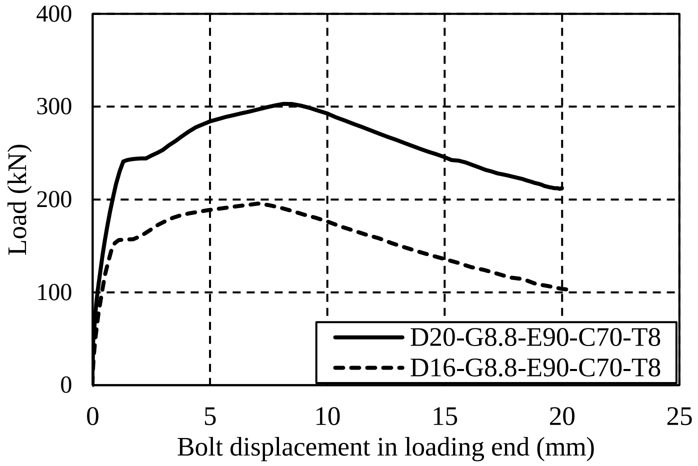

Fig. 24. Influence of bolt diameter in EHB connections with high strength concrete.

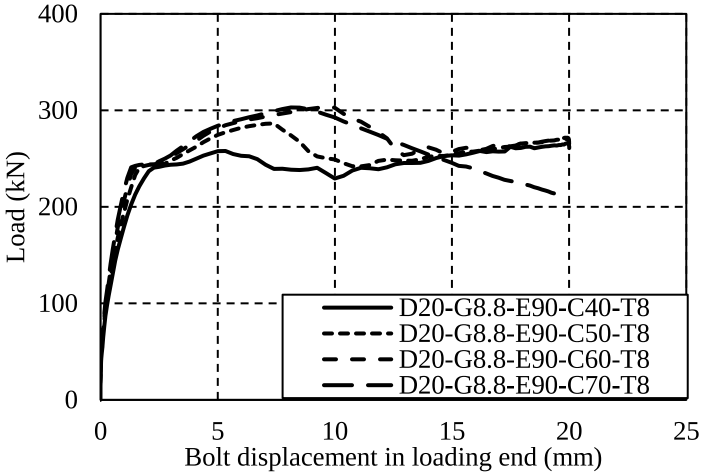

Fig. 25. Influence of concrete grade in M20 EHB connections.

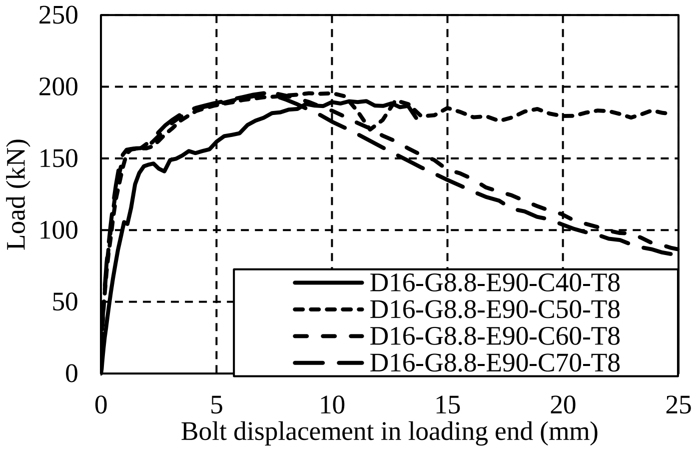

Fig. 26. Influence of concrete grade in M16 EHB connections.

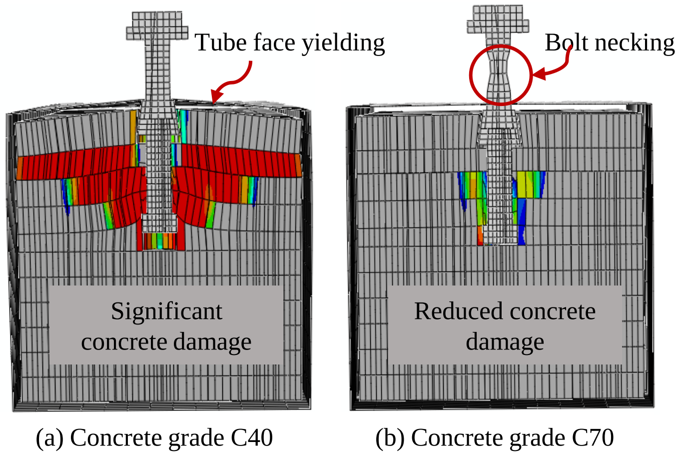

Fig. 27. EHB connection behaviour with different grades of concrete.

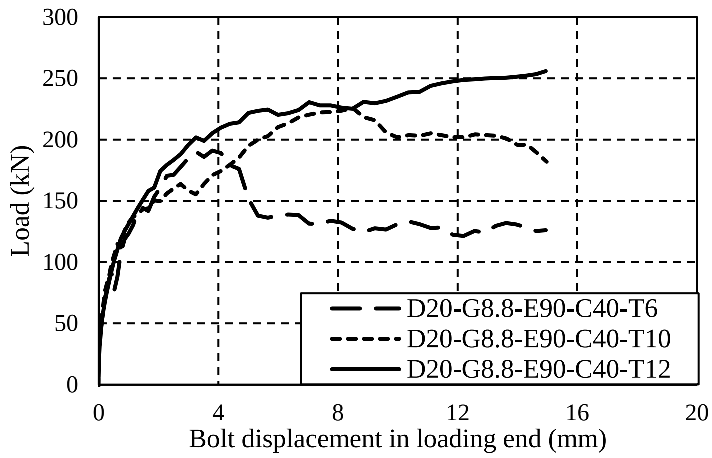

Fig. 28. Influence of tube thickness in EHB connections.

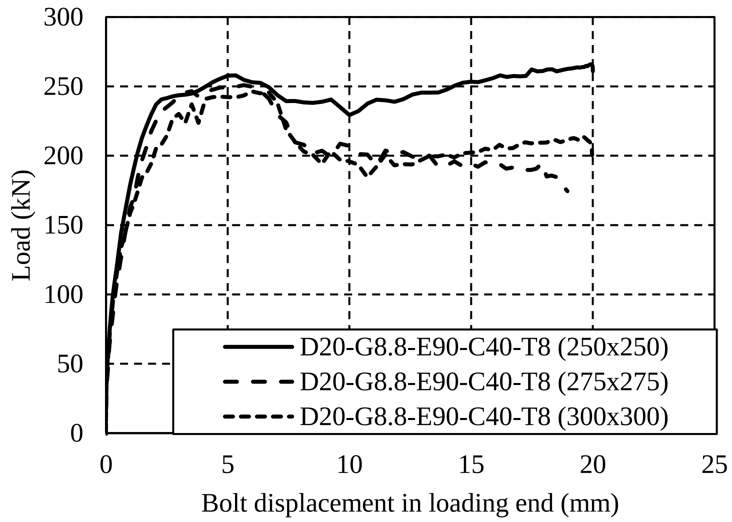

Fig. 29. Influence of cross-section dimension in EHB connections.

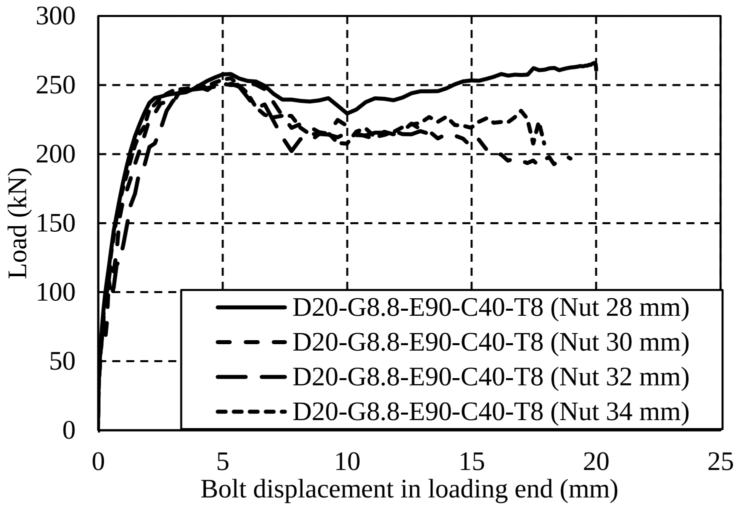

Fig. 30. Influence of bolt headed nut diameter in EHB connections.

Table 1: Summary of test data for hollow stub column tests adopted from Zhu *et al.* [24].

Specimen	Dimension, *B* or *Dia* (mm)	Section properties			Material Properties (N/mm^2)		
		T (mm)	B/t or D/t	L (mm)	f_y	f_u	E_s
CHS-1	200.3	5.96	33.6	695	452	581	216000
SHS-1	180 × 180	5.94	30.2	695	465.5	580	216500
OctHS-1	60	5.55	10.8	695	388.1	505.8	215000

Table 2: Summary of test data for CFST stub column tests adopted from literature.

Source	Specimen	Dimension, *B* (mm)	Section properties			Material Properties (N/mm^2)				
			T (mm)	B/t	L (mm)	f'_c	E_c	f_y	f_u	E_s
Huang *et al.* [25]	SU-040	200 × 200	5	40	840	27.15	N/A	265.8	N/A	N/A
	SU-070	280 × 280	4	70	840	31.15	N/A	272.6	N/A	N/A
Schneider *et al.*[26]	S2	127 × 127	4.34	29	609.6	26.05	24600	357	N/A	190200
	S4	127 × 127	5.67	22	609.6	23.80	23500	312	N/A	203900
	S5	127 × 127	7.47	17	609.6	23.80	23500	347	N/A	204600
Guo *et al.* [27]	S1-80-C-2	80.24 × 80.24	1.6	50.1	240	38.5	N/A	279.9	N/A	N/A
	S2-110-C-3	109.82 × 109.82	1.525	72	330	38.5	N/A	279.9	N/A	N/A
Sakino *et al.* [28]	CR-8-A-8	119 × 119	6.47	18.4	324	77	N/A	835	N/A	N/A
Han *et al.* [29]	sczs2-1-4	120 × 120	5.86	20.5	360	43.6	28740	321	N/A	N/A
	sczs2-2-3	140 × 140	5.86	23.9	420	36.6	26340	321	N/A	N/A
	sczs2-3-2	200 × 200	5.86	34.1	600	11.76	N/A	321	N/A	N/A

Table 3: Summary of test data for blind bolted pull-out tests adopted from literature.

Source	Specimen	Column geometry	*B* (mm)	Column section properties				Material Properties of steel tube and concrete (N/mm^2)					Blind-bolt details					Bolt material properties (N/mm^2)			Other information	
				t (mm)	B/t	H (mm)	t_p (mm)	f'_c	E_c	f_y	f_u	E_s	Bolt Grade	Bolt[a]	D (mm)	Embed. Depth (mm)	Torque (Nm)	f_y	f_u	E_s	δ	ξ
Yao *et al.* [16]	T6_D16_N1_E	Circular	324	6	54	800	N/A	48	N/A	350	430	N/A	8.8	HABB	16	0	N/A	600	830	N/A	0.36	0.57
	T8_D16_N1_E	Circular	324	8	40.5	800	N/A	48	N/A	350	430	N/A	8.8	HABB	16	0	N/A	600	830	N/A	0.43	0.77
	T10_D20_N1_E	Circular	324	10	32.4	800	N/A	48	N/A	350	430	N/A	8.8	HABB	20	0	N/A	600	830	N/A	0.49	0.99
	T6_D16_N2_E	Circular	324	6	54	800	N/A	48	N/A	350	430	N/A	8.8	HABB	16	100	N/A	600	830	N/A	0.36	0.57
	T8_D20_N2_E	Circular	324	8	40.5	800	N/A	48	N/A	350	430	N/A	8.8	HABB	20	100	N/A	600	830	N/A	0.43	0.77
	T10_D20_N2_E	Circular	324	10	32.4	800	N/A	48	N/A	350	430	N/A	8.8	HABB	20	100	N/A	600	830	N/A	0.49	0.99
Agheshlui *et al.* [18]	A-1M16-Mid	Square	300	8	37.5	500	N/A	50	N/A	355	473	N/A	8.8	HABB	16	80	N/A	764	955	N/A	0.45	0.82
	A-1M20-Side	Square	300	8	37.5	500	N/A	50	N/A	355	473	N/A	8.8	HABB	20	80	N/A	790	990	N/A	0.45	0.82
	B-1M20-Side	Square	400	12.5	32	500	N/A	57	N/A	378	490	N/A	8.8	HABB	20	126	N/A	780	970	N/A	0.47	0.91
Xu *et al.* [30]	Oct-W150-T4-S	Octagonal	150	4	37.5	1600	25	N/A	N/A	436.3	544.7	19.8×10^5	10.9	SCBB	20	0	260	1118.4	1209.9	20.6×10^5	N/A	N/A
	Oct-W150-T8-S	Octagonal	150	8	18.75	1600	25	N/A	N/A	422.7	573.5	20.7×10^5	10.9	SCBB	20	0	260	1118.4	1209.9	20.6×10^5	N/A	N/A
Pitrakkos *et al.* [21]	HB16-100-8.8D-0-1	Square	240	20	12	N/A	25	0	0	N/A	N/A	N/A	8.8	HB	16	0	190	836	932	20.7×10^5	N/A	N/A
	HB16-100-8.8D-C40-2	Square	240	20	12	N/A	25	42.5	N/A	N/A	N/A	N/A	8.8	HB	16	0	190	836	932	20.7×10^5	N/A	N/A
	EHB20-150-8.8F-C40-2	Square	240	20	12	N/A	25	37.0	N/A	N/A	N/A	N/A	8.8	EHB	20	79	300	785	935	20.7×10^5	N/A	N/A

[a] HABB: Headed Anchored Blind Bolt; SCBB: Slip Critical Blind Bolt; HB: Hollo Bolt; EHB: Extended Hollo Bolt. *N/A refers to values that are not available in the article.

Table 4. Comparison of failure load between experiment, EC4 and FE analysis for square CFST stub columns.

Specimen	Experiment failure load, P_{test} (kN)	Full plastic resistance, N_{Pl} (kN)	FEA failure load, P_{FEA} (kN)	P_{test}/N_{Pl}	P_{test}/P_{FEA}
SU-040	2365.8	2305.4	2345.8	1.02	1.00
SU-070	3420.2	3508.4	3273.8	0.97	1.04
S2	1106.6	1118.5	1105.7	0.98	1.00
S4	1224.9	1226.4	1175.5	0.99	1.04
S5	2044.2	1949.1	1886.5	1.04	1.08
S1-80-C-2	144.6	146.8	138.1	0.98	1.04
S2-110-C-3	145.2	143.5	146.9	1.01	0.98
CR-8-A-8	3234.2	3297.9	3285.4	0.98	0.98
sczs2-1-4	1403.0	1470.0	1405.8	0.95	0.99
sczs2-2-3	2008.0	1903.5	1952.6	1.05	1.02
sczs2-3-2	2007.4	1877.6	1938.2	1.06	1.03
			Mean:	1.002	1.017
			CoV:	0.035	0.03

Table 5. Comparison of FEA ultimate load with experimental ultimate load for bolt tensile pull-out tests.

Specimen	Experiment ultimate load, P_{test} (kN)	FEA, P_{FEA} (kN)	P_{test}/P_{FEA}	FEA failure mode
T6_D16_N1_E	99	104	0.95	Bolt pull-out and tube wall yield
T8_D16_N1_E	144	152	0.94	Bolt pull-out and tube wall yield
T10_D20_N1_E	217	237	0.91	Bolt pull-out and tube wall yield
T6_D16_N2_E	149	147	1.01	Bolt necking
T8_D20_N2_E	240	215	1.11	Tube wall yield and bolt pull-out
T10_D20_N2_E	255	224	1.13	Bolt necking
A-1M16-Mid	151	152	0.99	Bolt necking
A-1M20-Side	242	246	0.98	Bolt fracture and no tube wall yield
B-1M20-Side	212	218	0.97	Bolt fracture
Oct-W150-T4-S	167	165	1.01	Localized deformation around hole
Oct-W150-T8-S	421	423	0.99	Bolt washer failure
HB16-100-8.8D-0-1	139	140	0.99	Sleeve failure
HB16-100-8.8D-C40-2	142	146	0.97	Bolt shank necking
HB20-150-8.8F-C40-2	227	223	1.01	Bolt shank necking
		Mean:	0.99	
		CoV:	0.06	